J. Fluid Mech. (1987), *vol.* 184, *pp.* 303–333
Printed in Great Britain

Velocity and vorticity distributions in periodic separating laminar flow

By D. S. MATHIOULAKIS AND D. P. TELIONIS
Department of Engineering Science and Mechanics, Virginia Polytechnic Institute and State University, Blacksburg, VA 24061, USA

(Received 5 February 1986 and in revised form 10 March 1987)

Steady and unsteady velocity components over a backward-facing circular arc are measured by laser-Doppler velocimetry. A periodic disturbance is added to the mean flow and the response of unsteady separation is investigated. Special attention is given to the distribution and the flux of vorticity.

1. Introduction

Aerodynamicists are interested in the phenomenon of separation because it controls the efficiency of lifting surfaces as well as the behaviour of separated flows and therefore phenomena like steady or unsteady stall. The study of unsteady separation has generated some controversies, mostly because of the widely varied tools of investigation and quite often because of confusing terminology. The significance of the phenomenon lies in its interaction with the entire flow field. Its properties may explain the local structure of the flow but these should only be viewed as a step towards the understanding and eventually the prediction of the global effects. In this paper we discuss our experimental efforts in this direction. We study how vorticity generated in the boundary layer is convected and shed. Also we examine the interaction of the separated free shear layer with the dead water and the rigid wall.

Experimental work on unsteady separation has been initiated in the past few decades, following the pioneering work of Sears (1956), Moore (1958) and Rott (1956). The experimental work of Vidal (1959) and Ludwig (1964) pertains only to steady flow, and the work of Despard & Miller (1971) is confined to high-frequency oscillatory flow. Our knowledge at the beginning of the 1970s about this complex phenomenon was therefore remarkably narrow and there was a serious need for more intensive experimental investigation. Some progress was achieved by methods of flow visualization, and by hot-wire-anemometer techniques. Such methods have been employed by Schraub *et al.* (1965), Wérlé (1973), Ruiter, Nagib & Fejer (1971) and McCroskey (1971) to study unsteady viscous flow phenomena. In a more recent effort, Carr, McAlister & McCroskey (1977) employed a variety of sensing devices, ranging from flow-visualization methods (tufts, smoke) to pressure or velocity measuring methods (pressure transducers, hot-wire anemometers, etc.) to study the phenomenon of unsteady stall. In the present study, pressure and velocity signatures throughout a period of oscillation are given for different stations on a backward-facing curved surface. The results are compared with flow-visualization data. In all the recent contributions, with the exception of Despard & Miller (1971), the specific cases considered and the scale of the models were designed for a study of the entire

flow field. The boundary layers were very thin and it was difficult to study the features of the unsteady boundary layer and, in particular, separation. Moreover, in most cases, the boundary layer was turbulent upstream of separation. Detailed investigations of the flow properties in the immediate neighbourhood of unsteady turbulent separation were reported by Simpson (1981).

The present group attempted to examine more closely the immediate neighbourhood of unsteady laminar separation. In the first phase of the work (Telionis & Koromilas 1978; Koromilas & Telionis 1980), emphasis was given to the qualitative aspects of the flow. This was accomplished by flow-visualization methods in water–glycerin mixtures to achieve thick boundary layers with not very small velocities. Steady flows over moving surfaces were first examined in an open channel. Unsteady effects, transient and oscillatory, were later investigated in a closed water tunnel designed and constructed for this purpose, with two different systems of pressure-disturbance generation. Later, Mezaris & Telionis (1980) obtained detailed laser-Doppler velocimetry (LDV) measurements over a rearward-facing circular arc. In this work, unsteadiness was introduced by a flap pulsating over the circular arc. The model employed in the present study is the same as that of Mezaris & Telionis and will be described in the main body of the paper.

Two very interesting pieces of work have appeared in the literature recently (Varty & Currie 1984; Didden & Ho 1985). Varty & Currie employed a one-component laser-Doppler anemometer to measure the velocity parallel to the wall and calculated the other component using the continuity equation. The present work goes beyond the accomplishments of Varty & Currie (1984) and Mezaris & Telionis (1980) by employing simultaneous, two-component measuring techniques and examining both steady and unsteady flows. The results are reduced and analysed in a manner similar to the one suggested by Varty & Currie. Didden & Ho studied the separation induced by periodically generated ring vortices in pulsed impinging jets. They employed hot wires and pressure transducers to create a complete documentation of the flow field. The work of Varty & Currie was concerned only with steady flow. In all the flows studied by Mezaris & Telionis (1980), Didden & Ho (1985) and the present authors, the flow is periodic. However, in the case considered by Didden & Ho, the separated region is swept away completely and then separation creeps back from downstream. This provided a unique case of downstream-moving separation which is very little understood and very difficult to capture in the laboratory. In the present report, the excursions of separation are small, and the periodic response of the free shear layer dominates the flow field.

It is well known that, for a flat plate, the velocity amplitude ratio is scaled by the frequency parameter $k = \omega x/U_\infty$, where ω, x and U_∞ are the frequency, the distance along the wall and the free-stream velocity, respectively (Lighthill 1954). With increasing k, the amplitude profiles have been proved analytically and experimentally (Telionis 1979; McCroskey 1977) to have smaller overshoots, while the maxima approach the wall. The oscillatory part of the flow tends to become plug flow and the Stokes layer is confined closer and closer to the wall. This is not the case if the adverse pressure gradient increases with x (Mezaris & Telionis 1980; Mezaris *et al.* 1987). In fact, the data of Mezaris & Telionis indicate overshoots about 10 times larger than the amplitude of the outer flow.

In the present paper we introduce the disturbance in the oncoming stream rather than through a pulsating flap. We then examine more carefully the flow in the vicinity of separation by a more powerful data-acquisition system, which permits

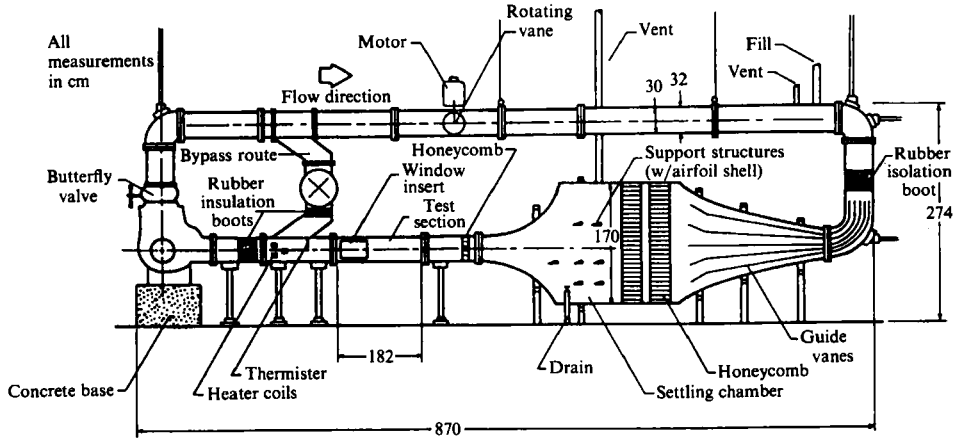

FIGURE 1. The VPI water tunnel showing the recent modifications. (*a*) A rotating vane drive by a variable speed motor; (*b*) a by-pass system with a control valve.

frequency domain analysis as well as Fourier series expansions of all waveforms. Also, the vorticity field is examined and instantaneous vorticity contours are displayed.

2. Facilities and the model

To conduct the research reported in this paper, some modifications and additions to our facilities were necessary. The basic task was to convert the tunnel to an unsteady water tunnel. To control the mean flow, a rotating vane was installed immediately above the test section as shown in figure 1. This vane was coupled to a HELLER d.c. motor with variable speed control. The unit automatically controls the speed to within $\pm 0.5\%$ of the set value. It is also equipped with an optical encoder which is interfaced directly with the laboratory computer.

A very significant factor in studies of unsteady aerodynamics is the amplitude of oscillation. To the knowledge of the present authors, in all facilities employing some mechanical method for control of the frequency of oscillation, the amplitude is a function of the frequency. A separate system is necessary if one desires to control independently both the amplitude and the frequency of the oscillation. In our case this was accomplished by a bypass pipe and a bypass valve as shown in figure 1. The position of this valve controls the efficiency of the rotating vane. Charts of the performance of these controls have been constructed (Telionis *et al.* 1986).

Any periodicity externally added to a tunnel generates free-stream turbulence. Many existing unsteady-flow facilities operate with turbulence levels of the order of 1–2%. Careful studies require much lower turbulence levels. To calm the flow in our tunnel (Schubauer, Spangenberg & Klebanoff 1948; Dryden & Abbott 1948; Loehrke & Nagib 1976; Wigeland, Ahmed & Nagib 1978; Tan-Atichat, Nagib & Loehrke 1982; H. M. Nagib 1984, private communication), we installed in the settling chamber a second set of finer honeycombs and three sets of fine screens. The periodic disturbance generated by the rotating vane ranges in amplitude from 3 to 17% peak to peak and in frequency from 0.2 to 8 Hz. The lowest turbulence level measured by a laser-Doppler velocimeter was about 0.4%.

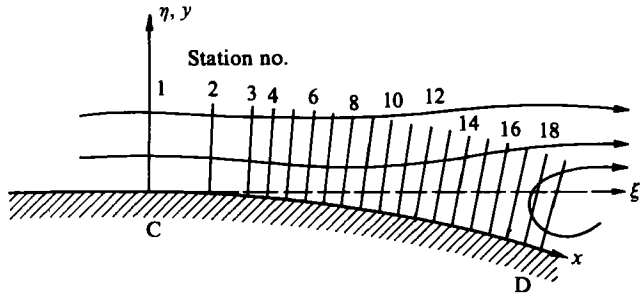

FIGURE 2. The circular arc with the two coordinate systems and 19 measuring stations. The distance between two stations on the wall from 3 and on is 5 mm. The radius of the circular arc is 450 mm.

Experiments were conducted on a model similar to that of Mezaris & Telionis (1980) and Mezaris *et al.* (1987). A convergence of the test section led the flow between two flat plates, which are slightly diverging to account for the two growing boundary layers. At the entrance of the convergence, the boundary layers growing on the walls of the tunnel were sucked. New boundary layers started developing on the convergence. Measurements on the walls of the flat plates indicate (Mezaris & Telionis 1980) that the laminar boundary layers are very nearly Blasius layers. Further downstream, the top surface diverged to generate a region of adverse pressure gradient. The bottom plate continued straight. In this way the separated region was not affected by mirror-image separation. It is recalled that flows about symmetric bodies, for example a circular cylinder, are controlled by the interaction of two shear layers with opposite signs of vorticity, which eventually lead to periodic shedding of large-scale vortices. The situation is different in the case of an airfoil at an angle of attack, whereby the separating flow over the suction side develops with little or no influence of the trailing-edge vorticity. This is exactly the type of flow simulated by our rig. Measurements were conducted on the diverging section which has the shape of a circular arc as shown schematically in figure 2.

Three-dimensional effects play a significant role in the phenomena under consideration. For a careful experimental study, it is imperative to address two basic issues, mainly (i) possible three-dimensional effects which the particular experimental rig introduces but which are foreign to the phenomenon under consideration; (ii) three-dimensional effects that are actually present in the problem under consideration, but owing to the design of the experiment are artificially eliminated.

To address the first issue, extensive measurements were obtained along the span of the model. In addition, dye visualization studies (Mathioulakis 1985) were conducted along planes parallel to the plane of symmetry. Both measurements and flow visualizations were triggered to provide phase-locked information for all phases of the periodic phenomenon. It was proved that three-dimensionality effects are confined to about 1.2–1.3 boundary-layer thicknesses next to the sidewalls. In the streamwise direction deviations of order 7% appear first at about 16–20 boundary-layer thicknesses downstream of the location of mean zero wall shear. The data reported in the present paper were obtained in a domain well within the two-dimensional region of the field.

Many recent contributions have appeared on the three-dimensional effects of separating flows over two-dimensional geometrical configurations. Mueller, Winkelmann and their associates (Arena & Mueller 1978; Winkelmann & Barlow 1980;

Winkelmann, Ngo & DeSaife 1982) have demonstrated that the line of separation itself it not straight and parallel to the generators of the model as one would expect. Instead, it displays a spatial periodicity which in oil visualizations resembles, and is known as, mushroom separation. Such phenomena were obtained on finite-span wings and it is possible that the three-dimensional effects are a response to the influence of the tips. Moreover, the wavelength is much larger than the distance from stagnation to separation. It is therefore believed that the basic two-dimensional mechanisms under investigation here control large portions of this type of separation as well.

Equally significant are three-dimensional phenomena which develop along the free shear layer, downstream of separation. Gerrard (1978) first reported the existence of three-dimensional structures in the form of 'knots' and 'fingers' in the wake of cylinders. Konrad (1976) and Bernal (1981) have also identified streamwise 'braid' structures in nominally two-dimensional free shear layers. Ho & Huerre (1984) suggest that such phenomena initially develop as two-dimensional instabilities (Michalke 1965), which later amplify to a level which brings them into a region of three-dimensional instabilities. A very careful study of the phenomenon was most recently reported by Wei & Smith (1986). Apparently, such three-dimensional phenomena are inescapable. However, they develop many boundary-layer thicknesses downstream of separation. Wei & Smith report a distance of about 0.2 cylinder diameters which even for Reynolds numbers as low as 10^4 corresponds to at least 10 boundary-layer thicknesses.

There is also some analytical evidence (Smith 1985) that many types of major instabilities can be triggered in the neighbourhood of separation. Moreover, the Tollmien–Schlichting mechanism can change form to produce other types of instabilities by means of three-dimensionality (Hall & Smith 1984). However, all these mechanisms are two-dimensional and linear in character.

The present measurements were obtained in a region in which, based on all the studies cited above, steady flow should be nominally two-dimensional. Our findings indicate that unsteady flow in this region is also two-dimensional.

3. Instrumentation and data acquisition

A two-component LDV system was employed to measure two orthogonal velocity components. The system, shown schematically in figure 3, employs two sets of Bragg Cells for shifting two of the three beams by 40 and 60 MHz respectively. Light scattered from seeding particles is received in a backward-scattering mode. Silicon carbide particles with diameters of a few microns were used for seeding. This ensured a data rate of about 500 samples per s. As a result, the signal thus generated was practically continuous. Example of raw data in the form of a time record will be presented and discussed in the next section. A single photo-multiplier was then used and the signal was down-mixed and filtered to provide instantaneous Doppler signals for two velocity components. The three beams entering the test section were arranged in such a way that the two velocity components measured were inclined by approximately 45° with respect to the predominant direction of the flow, as shown in figure 4. The desired components were then calculated on-line by the laboratory computer.

A special system was designed and constructed for traversing the measuring volume via mirrors. Such a system should meet some basic requirements: (i) it should allow very accurately controlled displacements; (ii) it should permit the displacement

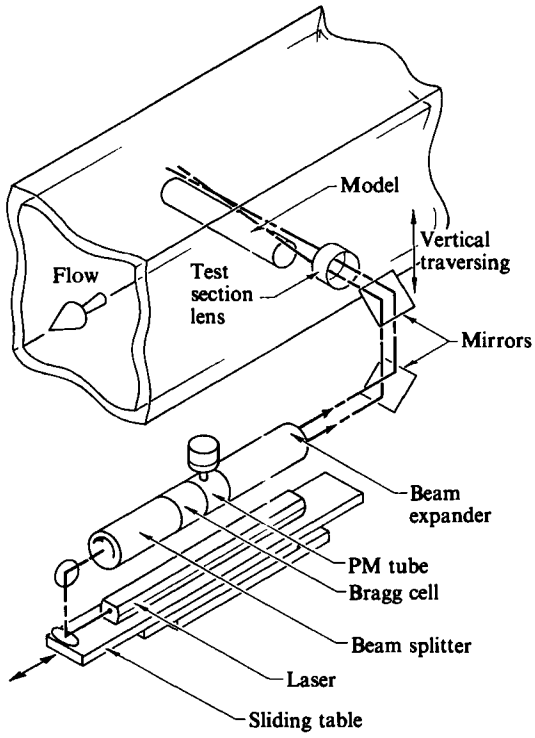

FIGURE 3. Sliding table and traversing mechanism.

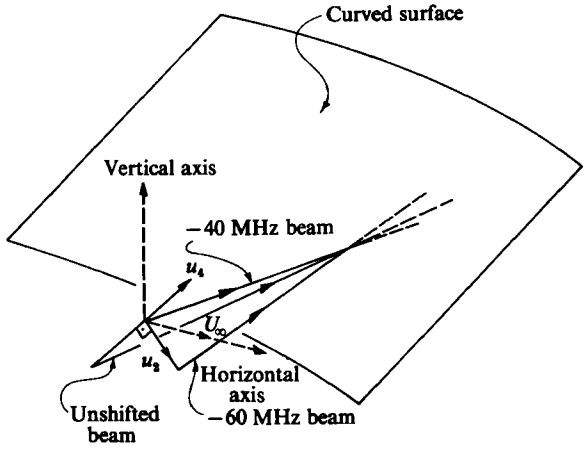

FIGURE 4. Schematic of the three laser beams over the circular arc and the velocity components obtained by them (u_2, u_4).

of the measuring volume in two directions, parallel and perpendicular to the flow; (iii) it should be controlled directly by the laboratory computer; (iv) it should be free of vibrations; and finally (v) it should allow the rotation of the beams about their bisector, so that the accuracy of component measurements is consistent. The system we designed and constructed is shown schematically in figure 3. The train of TSI optics is mounted on a linear translator which allows the entire system to move in

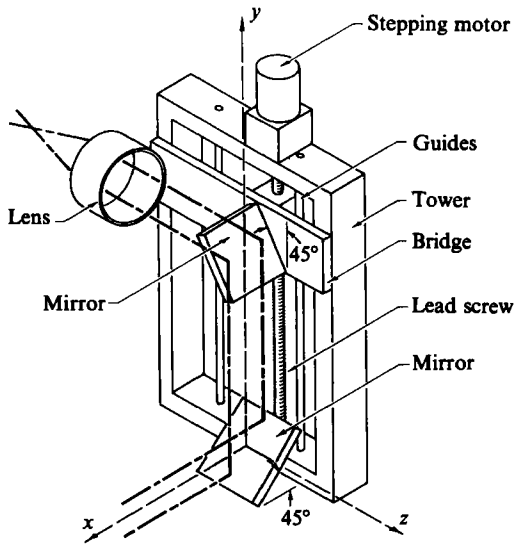

FIGURE 5. Detail of the traversing mechanism.

the x-direction. The parallel beams are then reflected twice from mirrors as shown in the figure and pass through a lens to converge at the measuring volume. The arrangement is very forgiving, because the distances between the three beams are preserved regardless of the inclinations of the two mirrors. Thus the angle of crossing of the beams at the measuring volume is an invariant of optical-element setting. The upper mirror together with the lens translate in the vertical direction to facilitate motion of the measuring volume along the y-axis. Details of the mirror tower are shown in figure 5. Both motions are controlled by stepping motors interphased with the laboratory computer. In this way steps as small as 1/100 mm can be implemented. Moreover, successive steps Δx and Δy may displace the measuring volume along any inclined path.

The LDV signals are processed with TSI counters which are interphased directly to our laboratory computer. This computer (MINC-11) is the heart of the entire system. It controls all other instruments, it displaces the measuring volume, it checks continuously for the quality of the signal, it receives the data, it manipulates them on line and it stores them. The particular arrangement for the present project is shown schematically in figure 6. An outline of the flow chart of this operation is shown in figure 7. The computer performs conditional averaging of the periodic signal and then orders the stepping motors to proceed to the next position in space. According to the specific application, the LDV counters are interrogated by the computer to ensure proper operation of the system. The software provides for input from encoders which ensure that the micropositioning commands have been executed properly.

The work described here was performed over a period of about four years. At first, measurements were obtained along verticals spaced 5 mm apart. Velocity components were then obtained successively. This phase of the work was reported in Telionis & Mathioulakis (1984). The majority of the data presented here were obtained along normals to the curved surface of the circular arc and at 19 streamwise stations (figure 2). In this phase of the work (Mathioulakis & Telionis 1985), two components of the velocity were measured simultaneously.

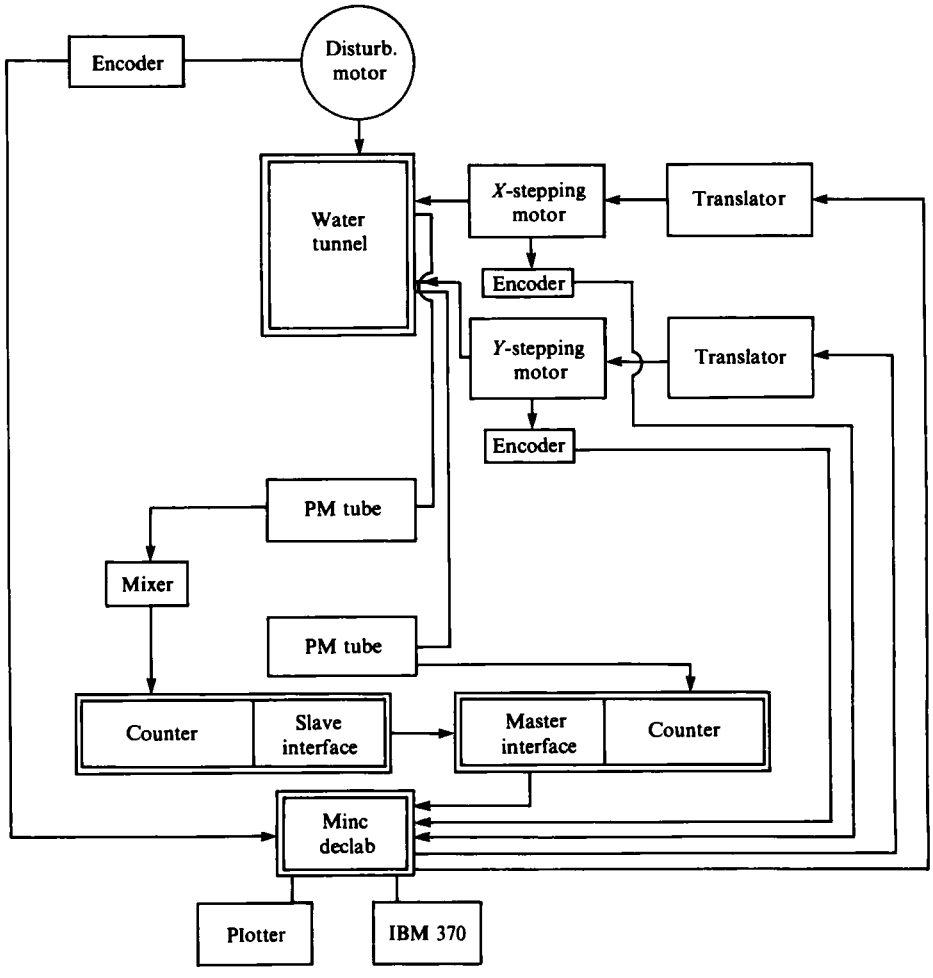

FIGURE 6. Arrangement of the equipment for obtaining and reducing the data.

The number of measuring points per station ranged between 30 and 60, while the smallest distance between two adjacent points was 0.2 mm. All the stations were located in the midspan region of the circular arc to ensure a two-dimensional flow field. The smallest distance along the wall between two stations was 5 mm, which corresponds to an angle of 0.011 rad. At each station, measurements were obtained in sequence, starting from the free stream and moving towards the surface of the model. The distance between two measuring points in the outer flow was about 1/10 of the boundary-layer thickness. Inside the boundary layer, the measuring grid was thickened in order to capture the details of the velocity gradient changes.

The measurements at a particular station came to an end when the probe volume touched the surface of the model, which was accompanied by an abrupt increase of the signal noise level. In this way, we were able to define the distance of the surface from the previous measuring point with an accuracy equal to the smallest displacement, which for this sequence of measurements was 0.2 mm.

The free stream was oscillated with a non vanishing mean and the period of oscillation was fixed at $T = 4.8$ s. This quantity was used to non-dimensionalize time.

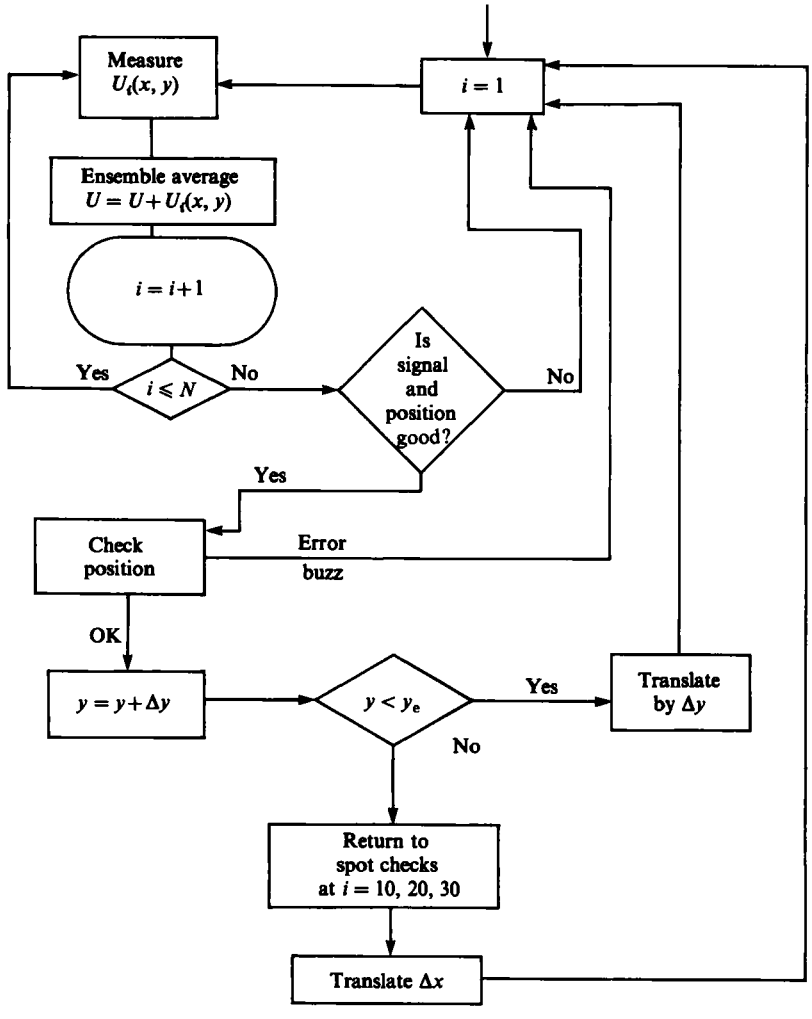

FIGURE 7. Flow chart for data acquisition.

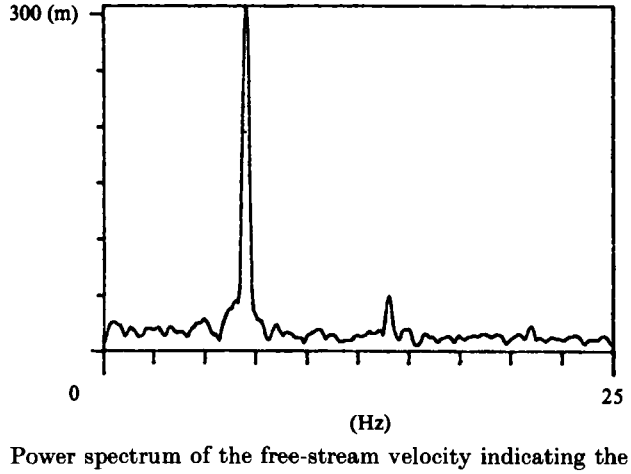

FIGURE 8. Power spectrum of the free-stream velocity indicating the driving frequency.

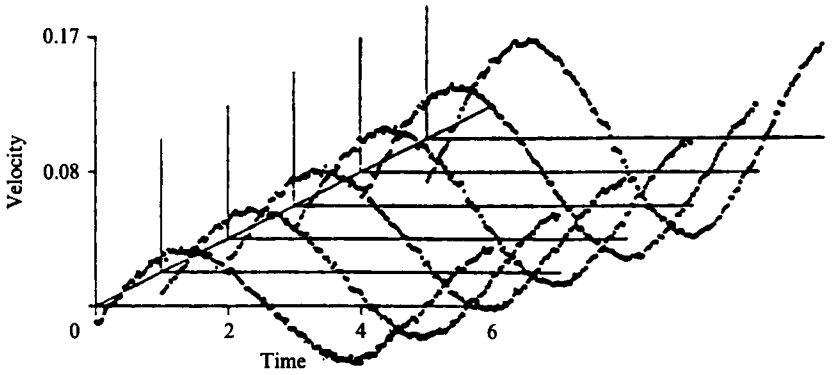

FIGURE 9. Selected velocity waveforms at $x = 50$ mm. Front to back correspond to $y = 6$, 5.2, 4.8, 4.2, 3.8 and 2.8 mm.

The mean value of the free-stream velocity U_∞ was 16.5 cm/s. Based on the radius R of the circular arc, the mean Reynolds number Re_m was 7.1×10^4, while the frequency parameter $\omega R/U_\infty$ was 3.57. The waveform of the flow was very nearly sinusoidal for the range of the possible disturbing frequencies. A power spectrum of the signal is shown in figure 8. Clearly, the second harmonic is hardly detectable.

The tunnel velocity may slowly drift and, on occasion, within a few hours deviated by 5% from the original setting. To ensure uniformity and eliminate the lowest-frequency disturbances in the free stream, the tunnel velocity was monitored by a third LDV channel, essentially playing the role of a free stream Pitot tube, which however provided a time-resolved signal.

The initiation of data acquisition was triggered by a pulse sent to the laboratory computer at a fixed opening of the rotating vane. The LDV signals were then conditionally averaged. For each velocity component, 160 instantaneous values per period were stored.

The reader will find extensive documentation of the data acquisition system in Mathioulakis (1985).

4. Results and discussion

Two coordinate systems were used: curvilinear orthogonal (x, y) with its x-coordinate aligned with the surface of the model and Cartesian (ξ, η), where ξ was parallel to the free stream (see figure 2). The velocity components in the (x, y)-system were denoted by u, v where u was parallel to the wall, while in the (ξ, η)-system the components were denoted by U, V where U was parallel to the free stream. The station $x = 0$ (or $\xi = 0$) corresponds to the joint of the flat plate with the circular arc. Waveforms of velocity at different elevations constructed of raw digital data are presented in figure 9. It is apparent that the digital data generate a nearly continuous signal. These waveforms are again very nearly sinusoidal. To demonstrate this, the experimental records were analysed by an FFT routine. This routine returned the mean value $\bar{U}$, as well as the amplitude of each harmonic:

$$U(x, y, t) = \bar{U}(x, y) + \sum_{n=1}^{80} [a_n(x, y) \sin \omega_n t + b_n(x, y) \cos \omega_n t], \tag{1}$$

where $\omega_n = n\omega$. Since the terms $a_n(x, y)$, $b_n(x, y)$ for $n \geqslant 2$ were much smaller than

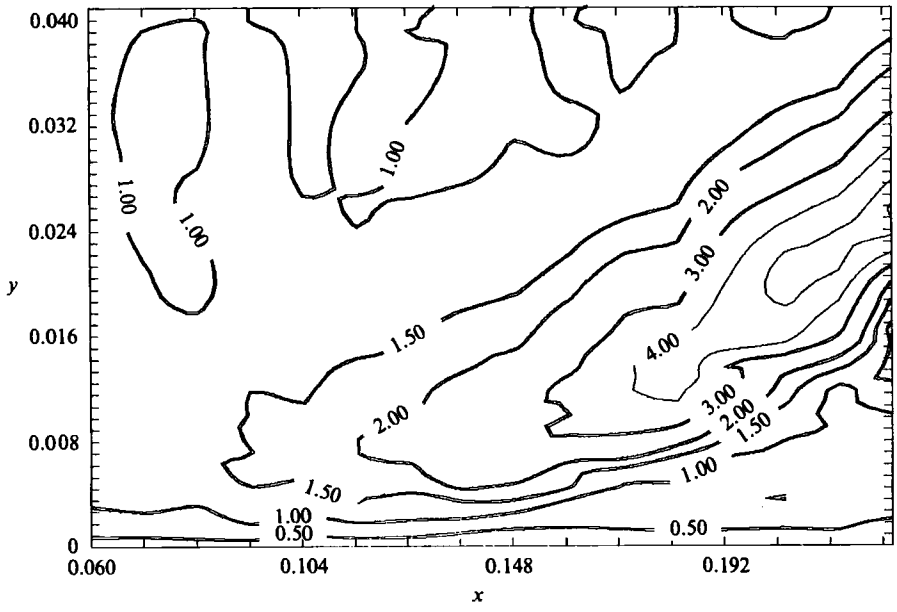

FIGURE 10. Contours of velocity amplitude normalized by local free-stream amplitude.

$a_1(x,y)$, $b_1(x,y)$ (less than 5%) here we present data only for the amplitude and the first harmonic

$$U(x,y,t) = \bar{U}(x,y) + a(x,y)\cos(\omega t - \phi), \tag{2}$$

where

$$\left.\begin{aligned} a(x,y) &= [a_1^2(x,y) + b_1^2(x,y)]^{\frac{1}{2}}, \\ \phi &= \tan^{-1} a_1/b_1. \end{aligned}\right\} \tag{3}$$

In figure 10, we show contours of constant amplitude a, non-dimensionalized by the local free-stream amplitude. The free-stream amplitude normalized by the free-stream mean velocity was 5%. In figure 10, we observe a classical feature of this type of flows: amplification of the oscillation as the boundary layer is penetrated. The amplification increases drastically as separation is approached. This was predicted numerically by Telionis & Romaniuk (1978) and experimentally by Mezaris & Telionis (1980). In the downstream direction, the peak of the amplitude moves away from the wall, in contrast to the case of oscillatory flow over a flat plate (Lighthill 1954), where the amplitude overshoots approach the wall for increasing $\omega x/U_\infty$. In our case, the amplitude overshoots downstream of separation are located within the free shear layer.

It is also observed that the overshoots are amplified continuously in the direction of increasing x, with a maximum value of 5 times larger than the local outer flow amplitude. Mezaris & Telionis (1980) reported overshoots about 10 times larger than the amplitude of the outer flow. This difference may be attributed to the fact that their disturbance was introduced locally into the flow.

Another characteristic feature of the flow is the change of the phase angle ϕ across the boundary layer. This is the phase difference between the local response and the free-stream velocity. In figure 11 we plot the variation of ϕ along y at 16 stations (3–18). We notice that close to the wall and at stations 11–18 (where the flow is reversed), there is a large phase lead (maximum value of 100°), while in the outer part

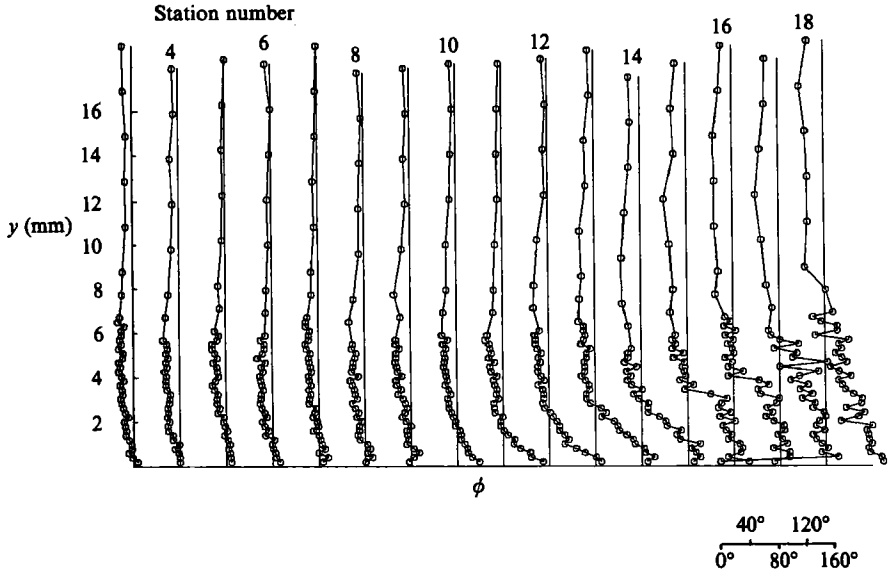

FIGURE 11. Profiles of phase angle between the local and the free stream velocity.

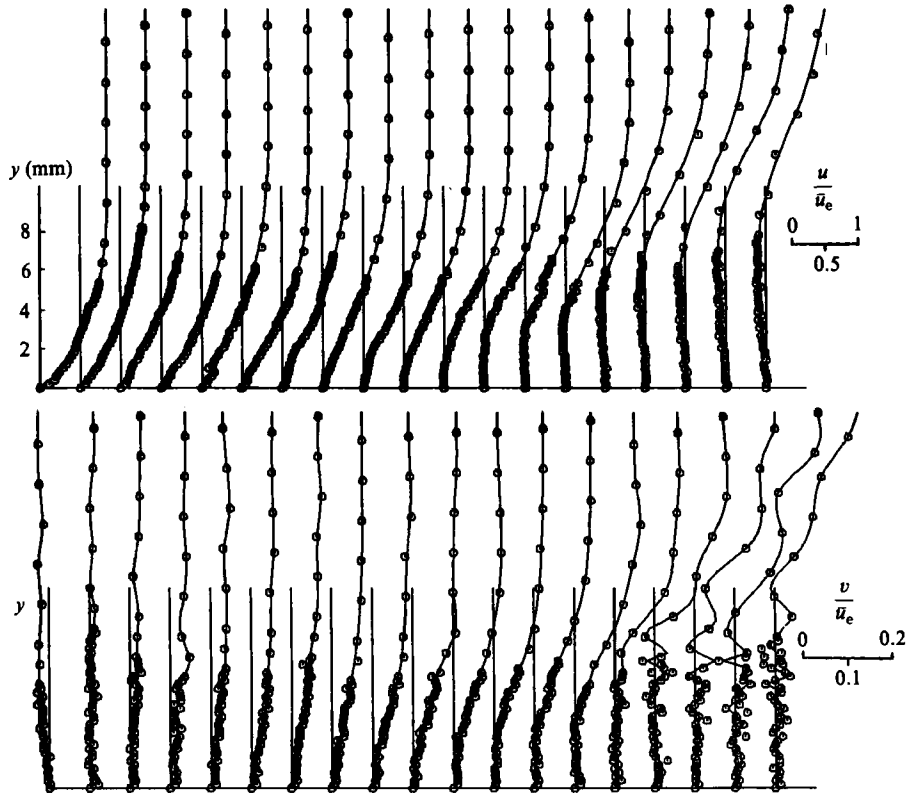

FIGURE 12. Velocity profiles, $t = \frac{1}{4}T$.

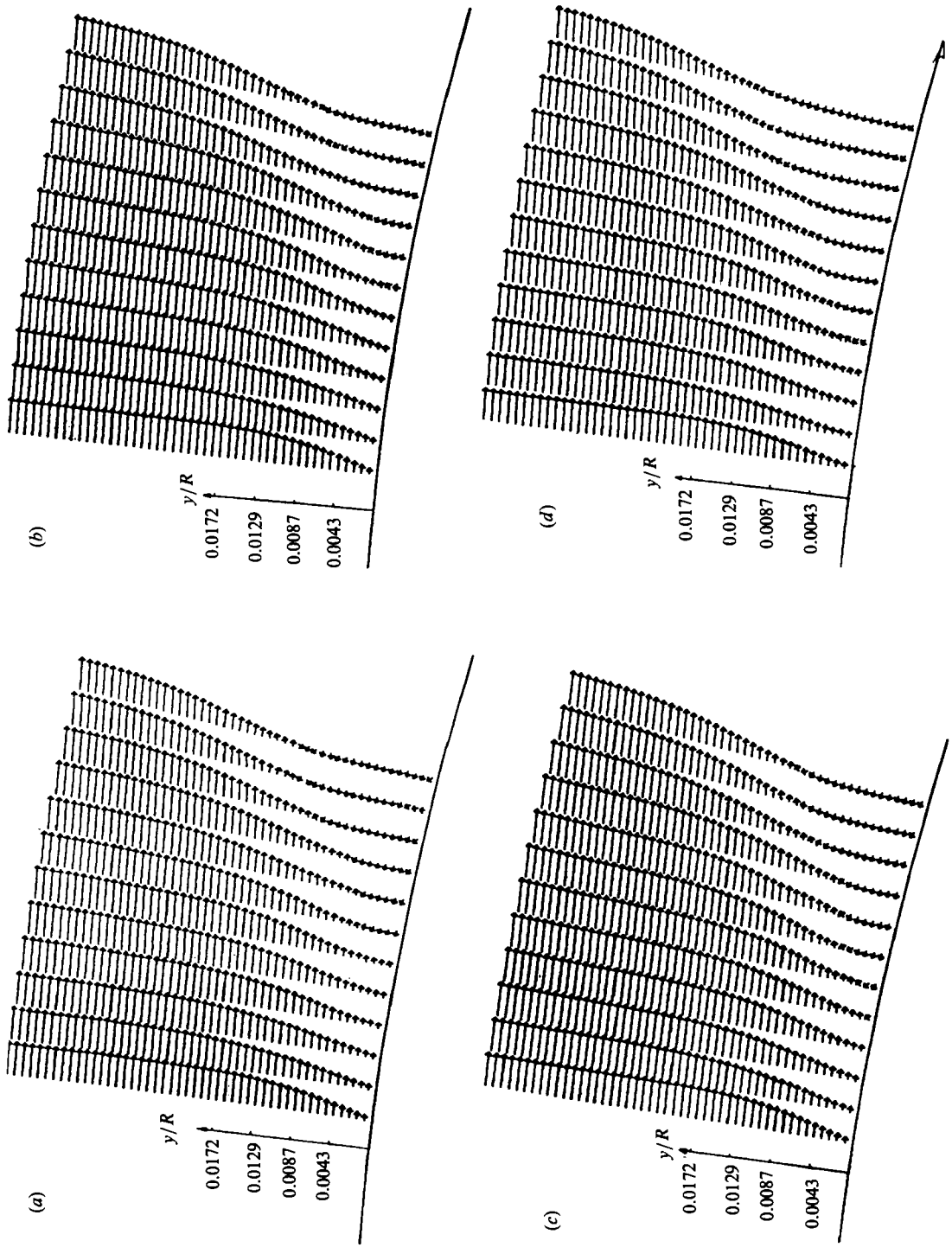

FIGURE 13. Vector field at instances within one period for stations 6–17. (*a*) $t = \frac{1}{4}T$, (*b*) $\frac{1}{2}T$, (*c*) $\frac{3}{4}T$, (*d*) T.

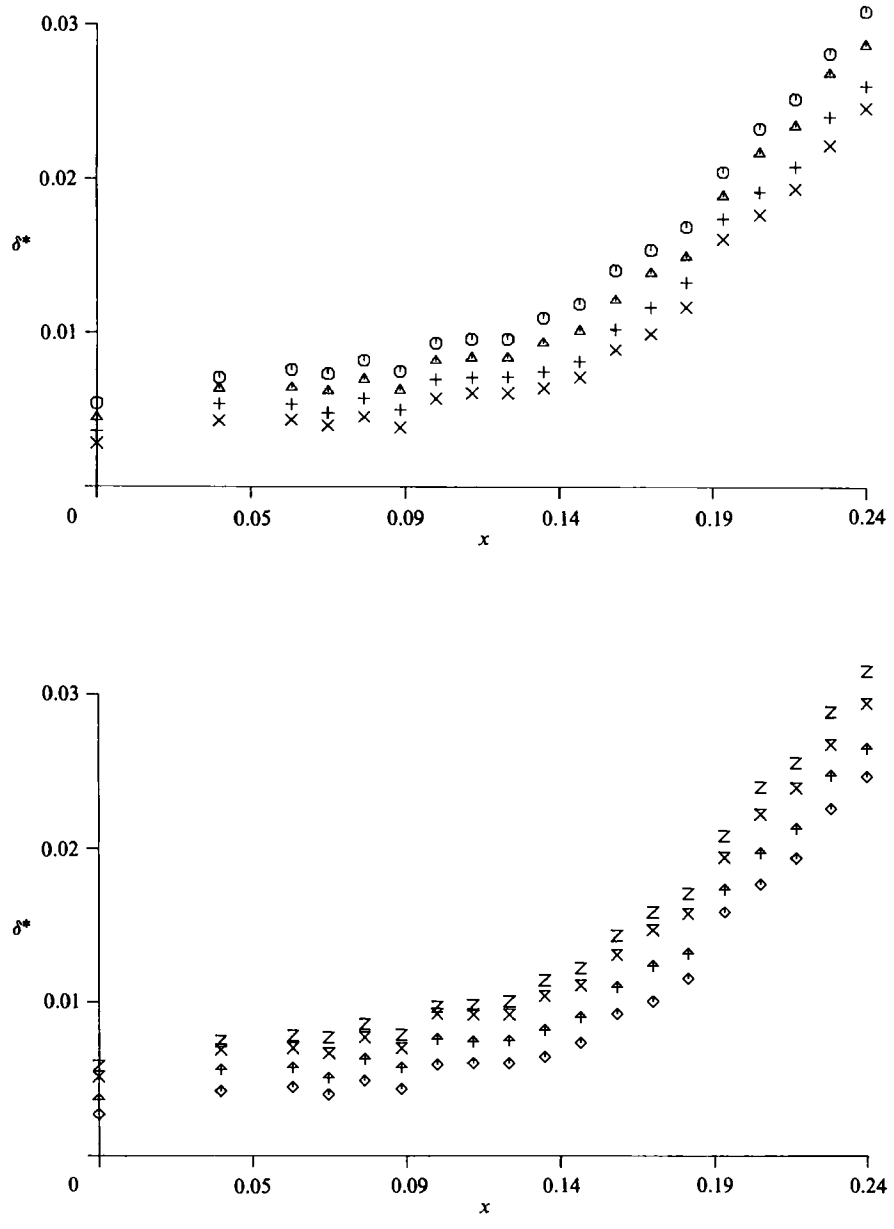

FIGURE 14. Displacement thickness as function of x, t. ⊙, $t = \frac{1}{8}T$; △, $\frac{1}{4}T$; +$\frac{3}{8}T$; ×, $\frac{1}{2}T$, ◇$\frac{5}{8}T$; ↑, $\frac{3}{4}T$; ⊼, $\frac{7}{8}T$; Z, $1T$.

of the boundary layer, there is a small phase lag (maximum absolute value of 20°). A simple explanation of this behaviour can be based on the fact that as we approach the wall, the inertia effects become less important compared to the pressure gradient. Tsahalis & Telionis (1974) reported a maximum phase lead of 45° and a phase lag of the order of 10° but they investigated numerically the flow upstream and up to separation only.

The velocity components parallel and perpendicular to the wall were normalized by the local time mean of the outer flow at the edge of the boundary layer $\bar{U}_e$. Then

they were smoothed in the y-direction by a cubic spline. Using the same routine we were able to obtain the smoothed velocity components at equispaced locations ($\Delta y = 0.4$ mm) in the y-direction. Their smoothed values u, v were used in our calculations for further reduction of the data. In figure 12 we show an example of raw data and the corresponding smoothed profiles. Figure 13 displays four instantaneous vector fields based on the smoothed u and v velocity profiles. A movie film has actually been prepared showing the variation of the velocity field in time. The film is available for loan upon request.

The boundary-layer thickness $\delta(x)$ was defined as the distance from the wall where u takes the value 0.95, while the displacement thickness δ^* was defined by the equation

$$\delta^*(x,t) = \int_0^\infty (1-u(x,y,t))\,\mathrm{d}y, \tag{4}$$

where all lengths were non-dimensionalized by the radius R of the circular arc. The above integration was performed over the smoothed profiles, using Simpson's rule. In figure 14 we show how δ^* changes in time at 19 stations.

Vorticity was calculated according to the formula

$$\omega = \frac{\partial u}{\partial y} + \frac{u}{1+y} - \frac{1}{1+y}\frac{\partial v}{\partial x}, \tag{5}$$

where ω was normalized by $\bar{U}_e/R$. Contours of constant vorticity $\omega/100$ are shown in figure 15 for eight time instants. The vortical layer fluctuates spacially, resembling a flapping tuft. The physical picture resembles a sheet which wraps around the body but separates from it at a point and periodically oscillates from then on, like a flapping flag. A more precise description of the phenomenon based on numerical calculations using the data obtained here follows in a later section.

5. Data processing

An attempt was made to evaluate the distribution of the static pressure in the flow field, by substituting the experimental velocity data in the Navier–Stokes equations. In polar coordinates, these are

$$\frac{\partial u}{\partial t} + \frac{u}{1+y}\frac{\partial u}{\partial x} + v\frac{\partial u}{\partial y} + \frac{uv}{1+y} = -\frac{\partial p/\partial x}{1+y} + \frac{1}{Re}\left[\frac{\partial^2 u}{\partial y^2} + \frac{1}{1+y}\frac{\partial u}{\partial y} + \frac{1}{(1+y)^2}\frac{\partial^2 u}{\partial x^2} + \frac{2}{(1+y)^2}\frac{\partial v}{\partial x} - \frac{u}{(1+y)^2}\right], \tag{6}$$

$$\frac{\partial v}{\partial t} + \frac{u}{1+y}\frac{\partial v}{\partial x} + v\frac{\partial v}{\partial y} - \frac{u^2}{1+y} = -\frac{\partial p/\partial x}{1+y} + \frac{1}{Re}\left[\frac{\partial^2 v}{\partial y^2} + \frac{1}{1+y}\frac{\partial v}{\partial y} + \frac{1}{(1+y)^2}\frac{\partial^2 v}{\partial x^2} + \frac{2}{(1+y)^2}\frac{\partial u}{\partial x} - \frac{u}{(1+y)^2}\right], \tag{7}$$

where

$$u = \frac{u^*}{\bar{U}_e},\quad v = \frac{v^*}{\bar{U}_e},\quad x = \frac{x^*}{R},\quad y = \frac{y^*}{R},\ t = \frac{\bar{U}_e}{R}t^*,\quad p = \frac{p^*}{\rho \bar{U}_e},\quad Re = \frac{U_e R}{\gamma}. \tag{8}$$

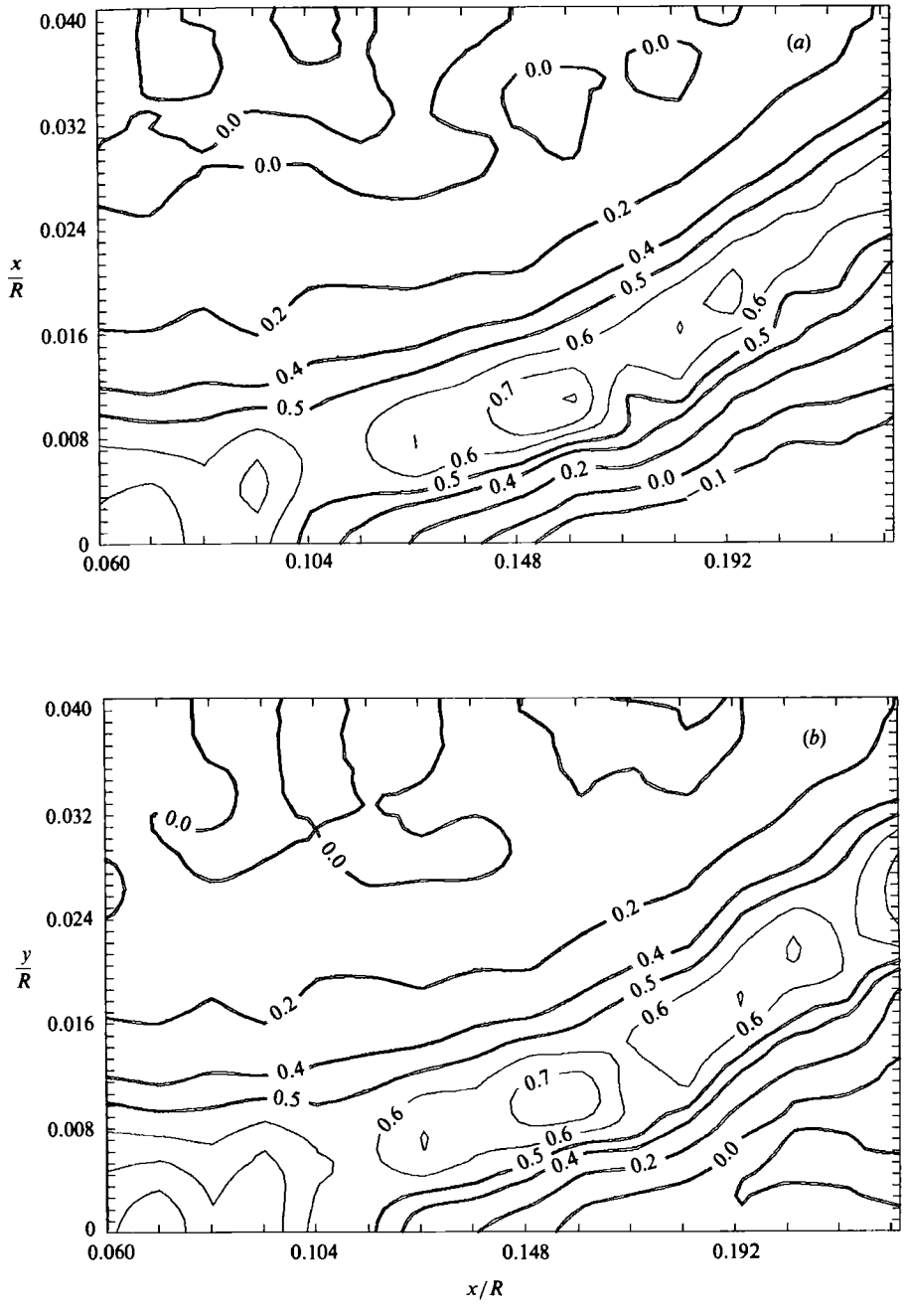

FIGURE 15(a, b). For caption see page 321.

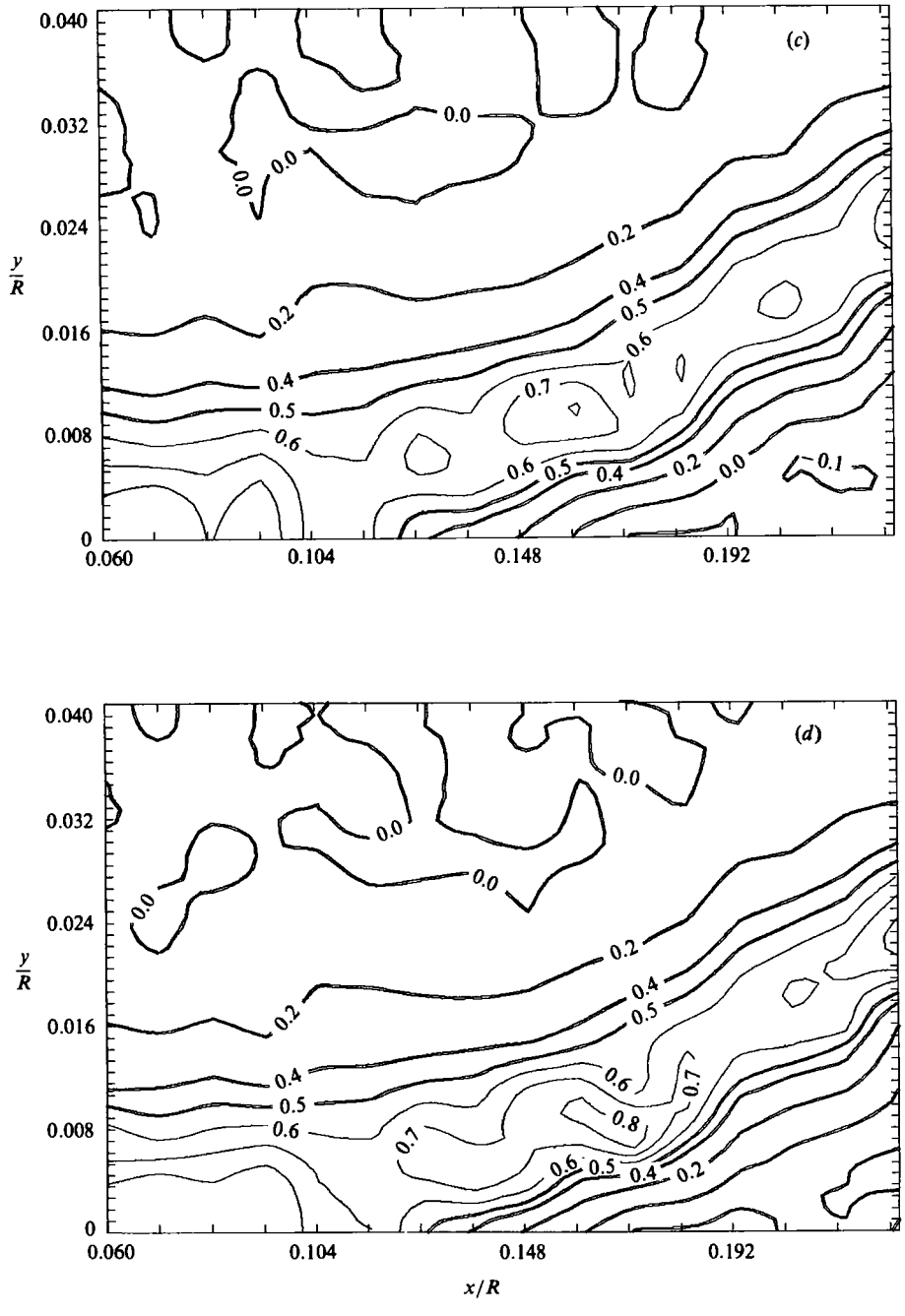

FIGURE 15(*c*, *d*). For caption see page 321.

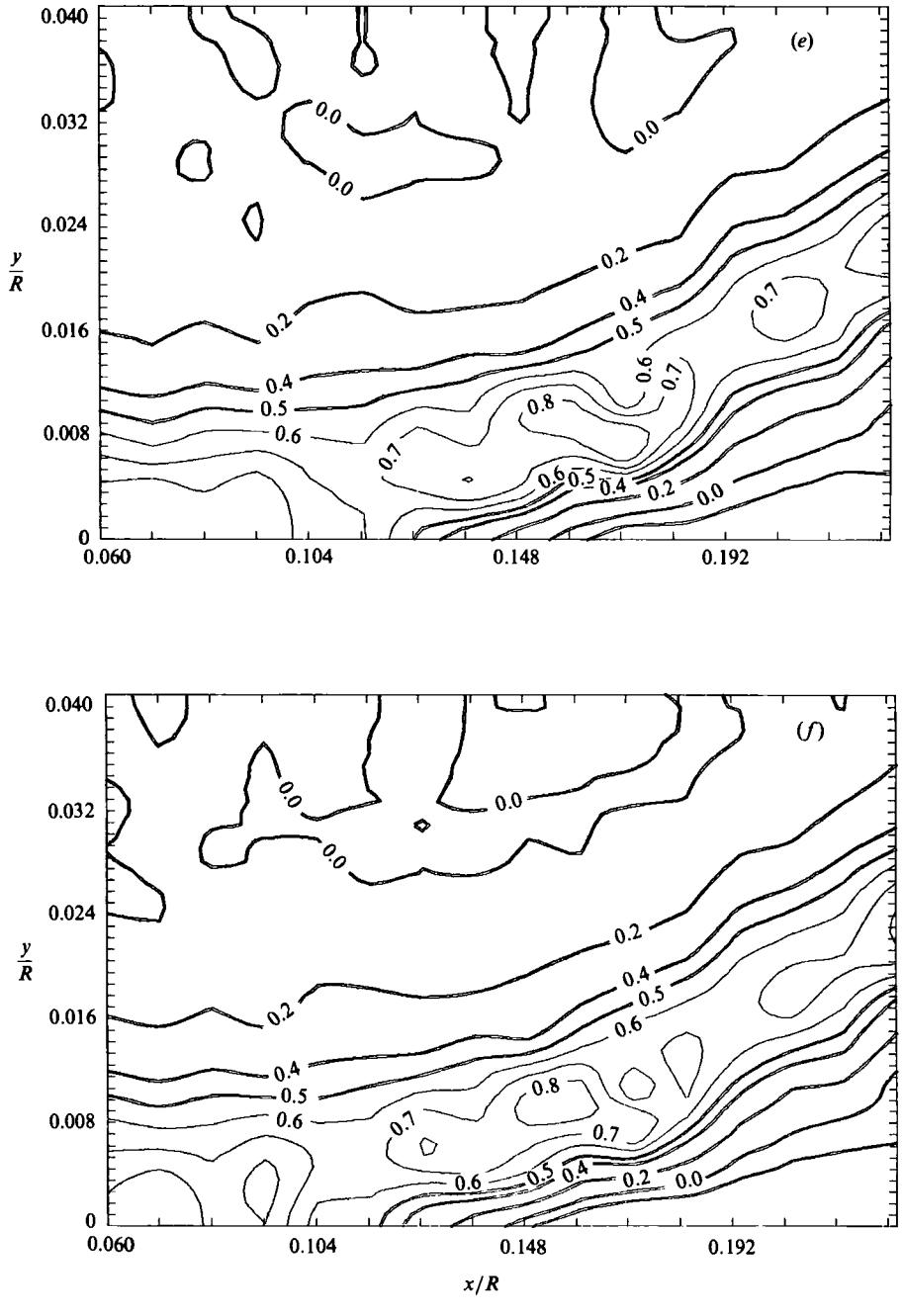

FIGURE 15(*e*,*f*). For caption see facing page.

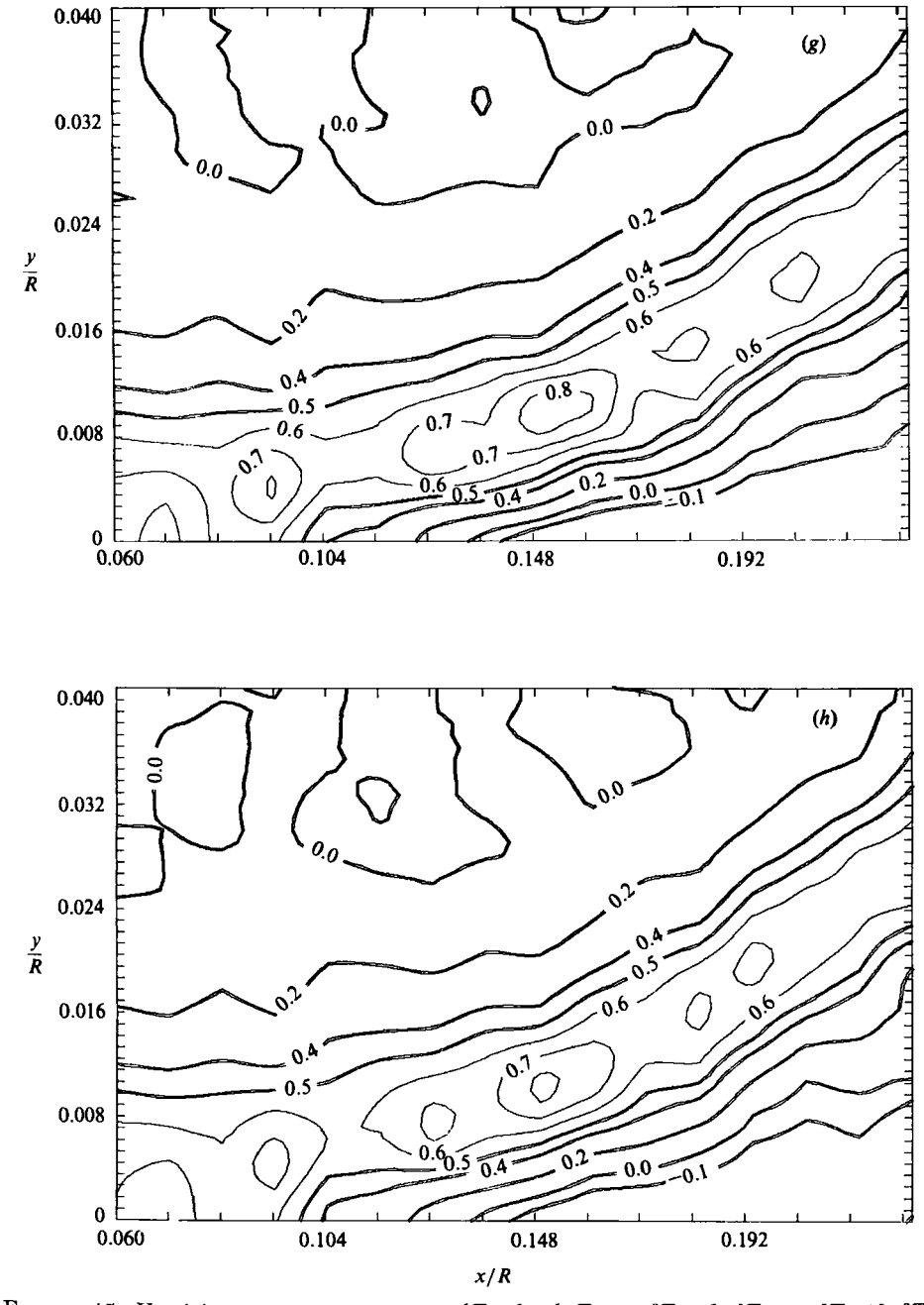

FIGURE 15. Vorticity contours at (*a*) $t = \frac{1}{8}T$, (*b*), $\frac{1}{4}$ T, (*c*) $\frac{3}{8}T$, (*d*) $\frac{1}{2}T$, (*e*) $\frac{5}{8}T$, (*f*) $\frac{3}{4}T$, (*g*) $\frac{7}{8}T$, (*h*) $1T$.

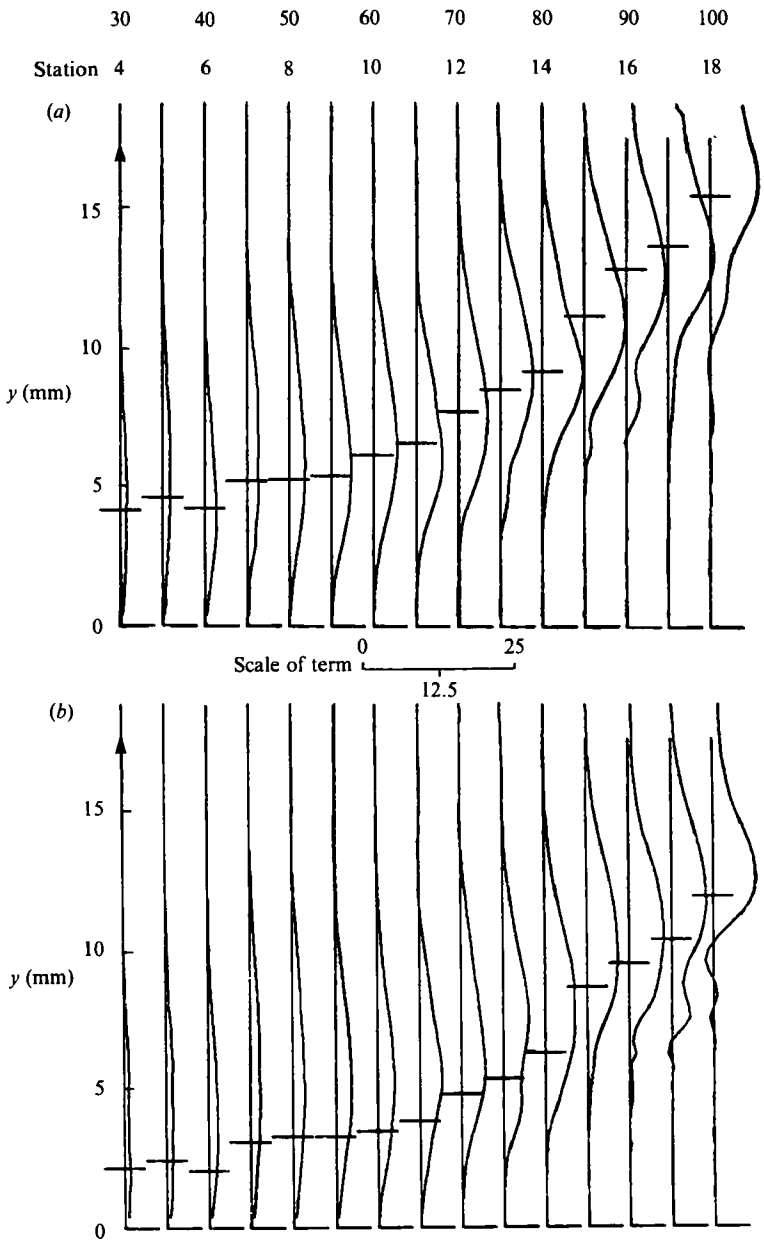

FIGURE 16. Profiles of $v\,\partial u/\partial y$ at stations 4–18. (*a*) $t = \frac{1}{2}T$, (*b*) T.

Symbols with an asterisk denote dimensional quantities. The derivatives of both components in the x- and y-directions have been expressed by central differences, and the time derivatives by forward differences. For example $\partial u/\partial x$ and $\partial u/\partial t$ were calculated by

$$\frac{\partial u}{\partial x} = \frac{u_{i,\,m+1,\,j} - u_{i,\,m-1,\,j}}{2\Delta x} \tag{9}$$

and

$$\frac{\partial u}{\partial t} = \frac{u_{i,\,m,\,j+1} - u_{i,\,m,\,j}}{\Delta t}, \tag{10}$$

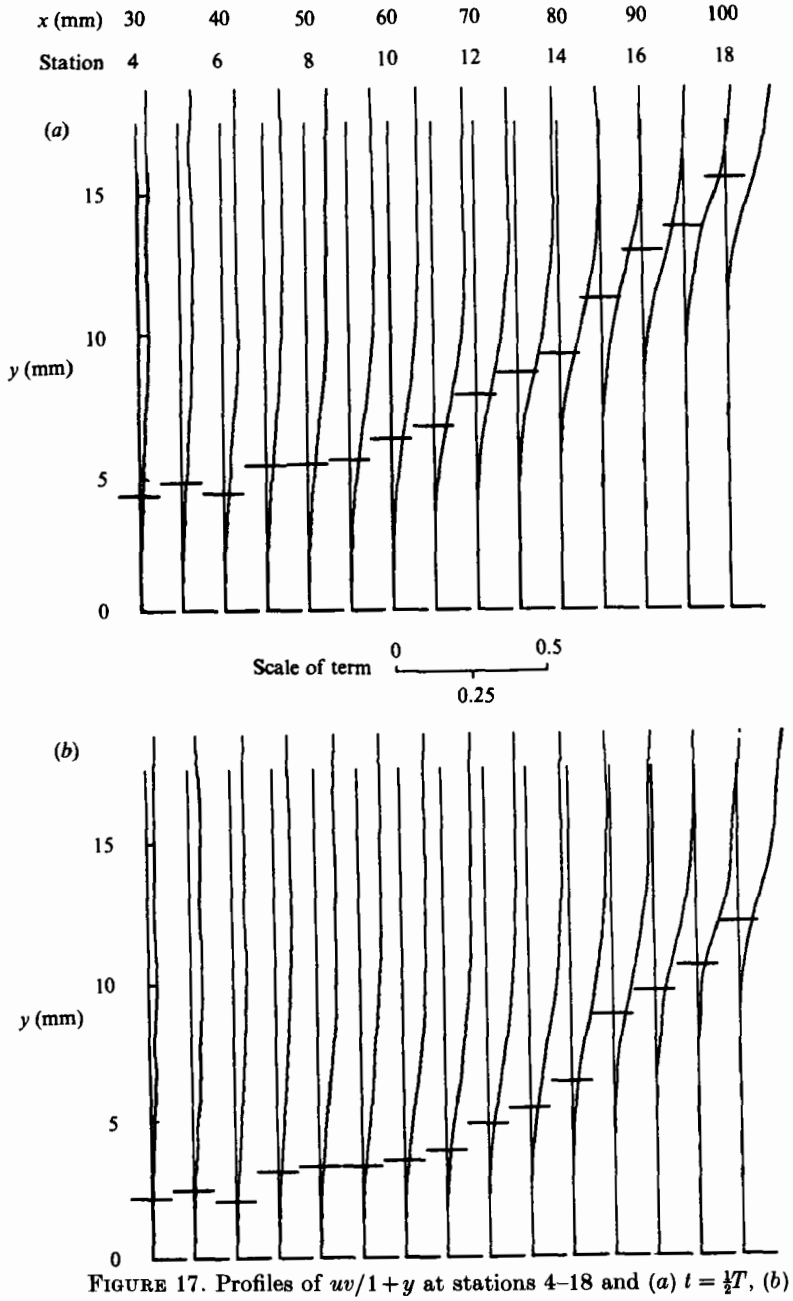

FIGURE 17. Profiles of $uv/1+y$ at stations 4–18 and (*a*) $t = \frac{1}{4}T$, (*b*) T.

where the symbols i, m, j represent the grid order of x, y and t, respectively. Some terms in (6) and (7) were of the order 10^{-3}–10^{-5}. We thus found from our experimental data that these equations can be written with great accuracy as

$$\frac{\partial u}{\partial t}+\frac{u}{1+y}\frac{\partial u}{\partial x}+v\frac{\partial u}{\partial y}+\frac{uv}{1+y}=-\frac{\partial p/\partial x}{1+y}+\frac{1}{Re}\frac{\partial^2 u}{\partial y^2}, \tag{11}$$

$$\frac{\partial v}{\partial t}+\frac{u}{1+y}\frac{\partial v}{\partial x}+v\frac{\partial v}{\partial y}-\frac{u^2}{1+y}=-\frac{\partial p}{\partial y}+\frac{1}{Re}\frac{\partial^2 v}{\partial y^2}. \tag{12}$$

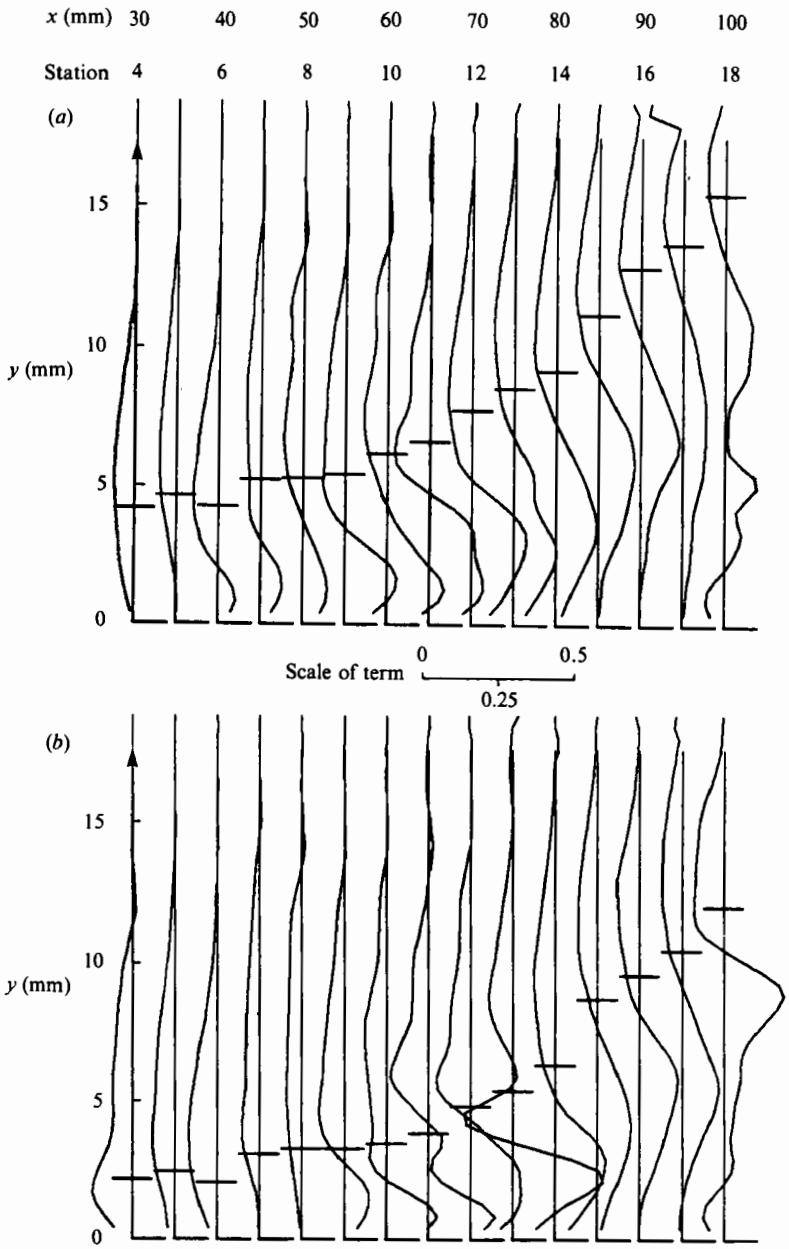

FIGURE 18. Profiles of $(1/Re)\ (\partial^2 u/\partial y^2)$ at stations 4–18 and (*a*) $t = \frac{1}{2}T$, (*b*) T.

In other words, the terms involving the second velocity derivatives, $\partial^2 u/\partial x^2$ and $\partial^2 v/\partial x^2$ are 3–4 orders of magnitude smaller, a finding which is in agreement with Varty & Currie (1984).

Examples of the profiles of terms of the above equations, for two time instants, $t = \frac{1}{2}T$ and T are shown in figures 16, 17 and 18. In these figures the instantaneous value of displacement thickness is marked by a short horizontal line segment for comparison.

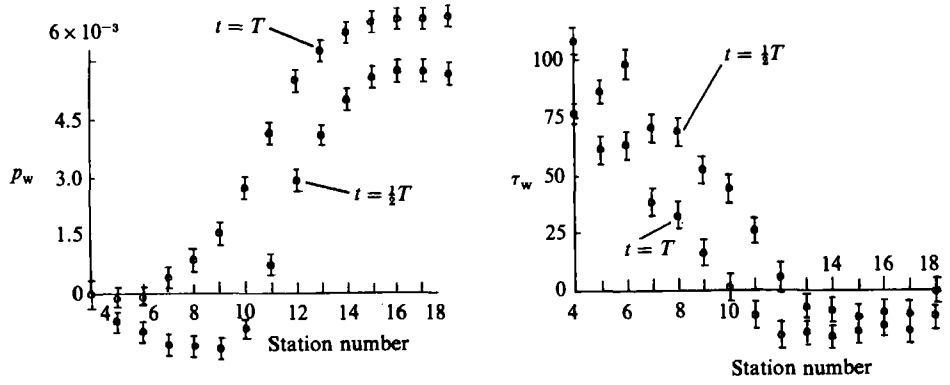

FIGURE 19. Wall pressure p_w and wall shear $\tau_w = \partial u/\partial y|_{y=0}$ at $t = \frac{1}{2}T$ (stations 4–18).

It should be emphasized here that discrepancies easily appear in this type of calculations. The quantity v is very small and very hard to measure. Moreover, x-derivatives are also small, and even harder to estimate. It turned out that errors as large as 20–30% were found in efforts to verify the validity of the continuity equation. Profiles of terms like $\partial u/\partial x$ appeared to be very irregular if estimated by differences in the x-direction. Instead, it was found that more consistent data could be obtained by estimating $\partial v/\partial y$ and then using the continuity equation to calculate $\partial u/\partial x$.

The term $\partial p/\partial y$ was then calculated from (12). This quantity is very small and as a result extremely small errors lead to erratic behaviour of corresponding profiles. Plots of $\partial p/\partial y$ are included in Mathioulakis (1985). The magnitudes of some quantities calculated are within the estimated error. Surprisingly, we noticed that most of the terms of the equations that we calculated appear more consistent near the wall. We noticed, for example, that $\partial p/\partial y$ is consistently negligible in the region $y \leqslant \delta^*$ upstream of the 14th station at $t = \frac{1}{2}T$ and upstream of the 12th station at $t = \frac{1}{6}T$. However, downstream of these stations (wake region) this does not hold.

Another example of the fact that near the wall, measurements and calculations were more consistent is the distribution of wall pressure. Employing (11) at $y = 0$, we can obtain the wall pressure p_w by integrating numerically the equation

$$\frac{\mathrm{d}p_w}{\mathrm{d}x} = \frac{1}{Re}\frac{\partial^2 u}{\partial y^2}\bigg|_{y=0}. \tag{13}$$

This integration was performed between stations 4 and 18. The error estimated in calculating these quantities was less than 10% of the largest displayed value. Apparently, the quantity $\partial^2 u/\partial y^2$ was estimated with greater accuracy near the wall than away from it. A further explanation of the quality of the data hinges around the technique of establishing the position of the wall with respect to the measuring volume, or equivalently the zero value of the measured quantities u and v. This was done by a linear extrapolation of the last three successful measurements before the laser beams hit the wall. This process was performed automatically by the computer. The variation of p_w along x at $t = \frac{1}{2}T$ and T is shown in figure 19 along with the variation of $\partial u/\partial y|_{y=0}$. Further smoothing is of course achieved by integration along the x-direction. We notice that p_w starts increasing three or four stations upstream of the point of zero skin friction.

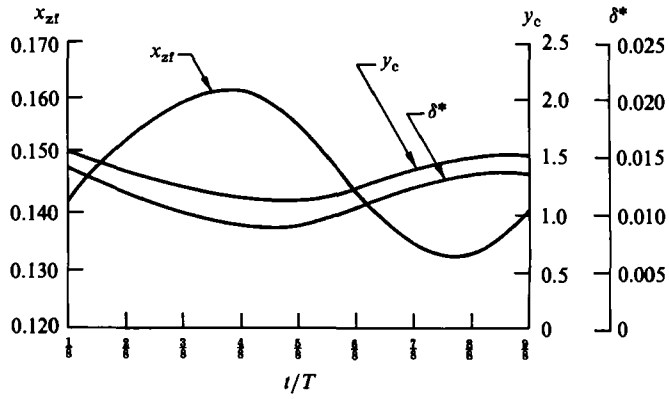

FIGURE 20. Time variations of the location of zero skin friction x_{zf}, the displacement thickness δ^*, and the centre of vorticity y_c.

6. Discussion

Separation is defined by aerodynamicists as the location on the surface of the body where the inviscid flow, the 'outer flow' in the terminology of inner and outer expansions, ceases to follow the body and turns into the main stream. This concept is meaningful only in the limit of $Re \to \infty$. For finite Reynolds numbers, the process is gradual and the above definition is ambiguous.

A variety of symptoms have been employed experimentally to signal separation (Sears & Telionis 1975; Williams 1977; Shen 1978; Cousteix 1986). Lacking a uniformly accepted definition of unsteady separation, experimentalists usually compare the behaviour of the symptoms. Didden & Ho (1985) specifically discuss the symptoms of (i) thickening of the boundary layer, (ii) ejection of vorticity and (iii) zero shear stress. They go one step further and find that the separation speed in the Moore–Rott–Sears (MRS) criterion, see discussion in Sears & Telionis (1975), equals the speed of the local peak of the displacement thickness. Their evidence also indicates that secondary vortex formation or the formation of a local shear layer is 'the generic flow module in the unsteady separation phenomenon'. The Didden & Ho experiments are special in character because they involve a pressure gradient which is favourable everywhere in the mean. Moreover, their displacement thickness has a maximum because their separated layer reattaches on the wall. In our case, and perhaps in all cases of massive separation†, there is some mean adverse pressure gradient and as a result, the displacement thickness grows continuously with downstream distance. There is no maximum.

The excursions of the point of zero skin friction are plotted in figure 20. In the same figure we plot for comparison the displacement thickness at the location of $x = 0.160$, which represents the fluctuations of the free shear layer. Skin friction leads the outer flow by about 45°. This is in agreement with earlier numerical findings (Tsahalis & Telionis 1974).

A parameter indicative of the validity of the boundary-layer assumption is the quantity $\bar{u}/\bar{v}$, the ratio of the two mean velocity components. Contours of this ratio are shown in figure 21(*a*). Asymptotic theories have recently indicated (see the review of Smith 1986) that in a coordinate system aligned with the displaced flow,

† Some authors prefer to use the term 'catastrophic' separation for separated regions that are not closed.

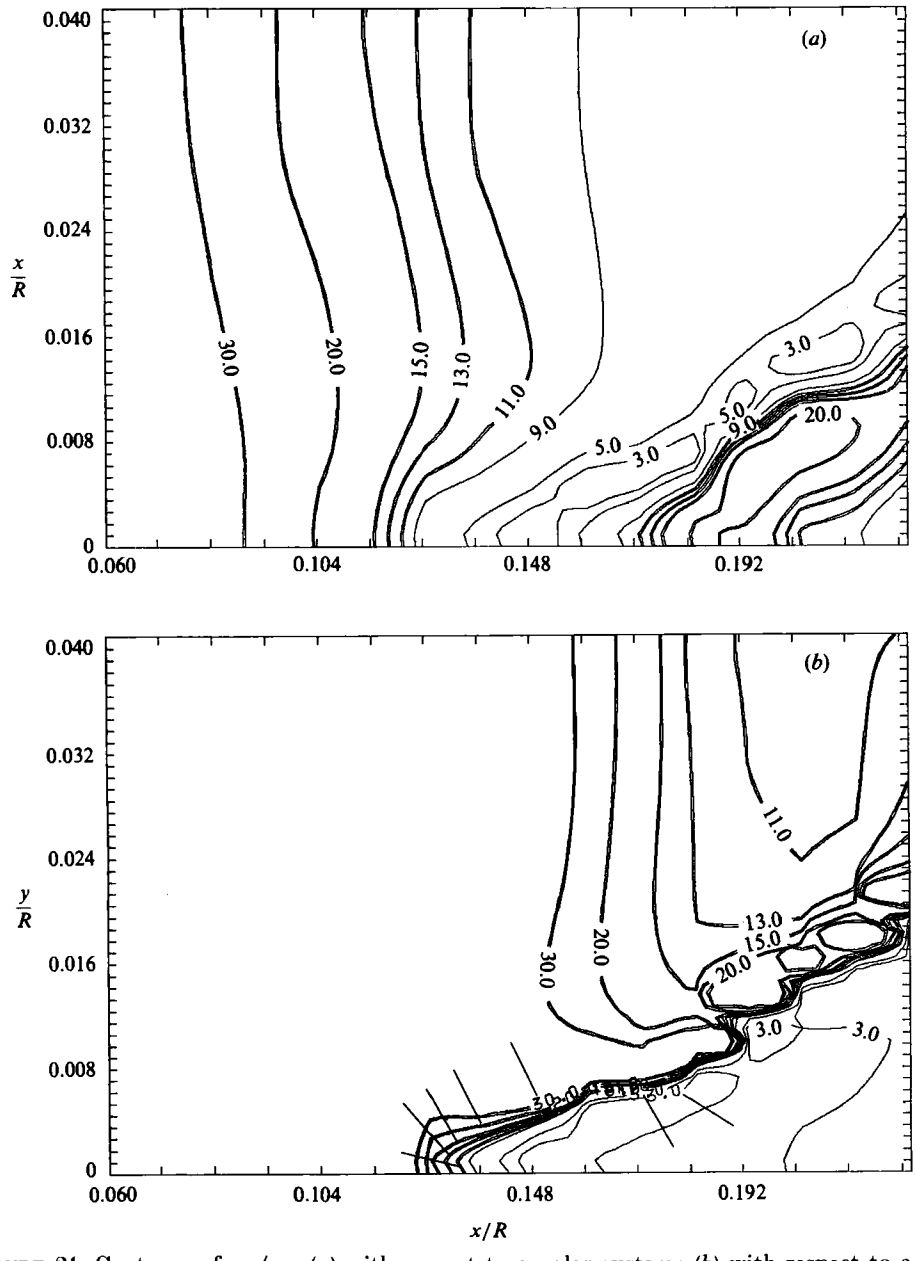

FIGURE 21. Contours of u_m/v_m. (*a*) with respect to a polar system; (*b*) with respect to a system aligned with the centre-of-vorticity curve.

the boundary-layer approximation is uniformly valid throughout separation. To demonstrate this we plotted in figure 21 (*b*) the $|\bar{u}/\bar{v}|$ ratio with respect to a coordinate system displaced off the body by the displacement thickness. The present data provide strong evidence in favour of the earlier asymptotic results. The ratio $\bar{u}/\bar{v}$ is very large along the attached boundary layer and the separating shear layer.

Asymptotic theories have concentrated on steady separating flow. Unsteadiness has been accounted for only in the form of hydrodynamic instabilities and their

possible growth (Smith 1985). It is therefore not possible to undertake a comparison with the present case, where the disturbance is introduced in the outer flow in a periodic fashion. However, a qualitative comparison is possible and turns out to be quite favourable. For example, theory predicts that the separation line for subsonic flow is concave upward (Smith 1986). This is clearly the case for our experimental data. Moreover, triple-deck theory predicts that the pressure levels off at a distance of approximately 8–9 units measured in terms of the stretched variable $X = Re^{3/8}(x-x_{sep})$. In the present case we estimate from figure 19 that in the mean, the pressure levels off at approximately the 15th station which was calculated to be $X \approx 7$.

A classical relationship between circulation Γ and vorticity Ω dictates that

$$\Gamma = \iint \Omega \, \mathrm{d}A, \tag{14}$$

where A is the area contained by the contour of integration of the circulation integral. Howarth (see discussion in Saffman & Schatzman 1982) has demonstrated that if the area is chosen appropriately, the rate of shedding of vorticity at separation becomes

$$\frac{\mathrm{D}\Gamma}{\mathrm{D}t} = \int_0^\delta \Omega u \, \mathrm{d}y, \tag{15}$$

which within the boundary-layer approximation yields

$$\frac{\mathrm{D}\Gamma}{\mathrm{D}t} = \tfrac{1}{2} u_e^2, \tag{16}$$

where u_e is the edge velocity at separation. This simple formula has been used extensively in the literature of discrete vortex dynamics.

Similar arguments have been presented by many theoreticians (for example, Birkhoff 1953; Clements 1973; Sarpkaya 1975; Saffman & Schatzman 1982) to estimate the strength of periodically shed vortex structures. Viewing the shedding process macroscopically, many experimentalists have indicated that (16) is not accurate. It was argued that in practice vorticity is shed at a considerably larger rate (Roshko 1953, 1954) but, on the other hand, the rate of vorticity shedding is decreased because of vortex annihilation (Fage & Johansen 1927). This is due to vorticity of opposite sign which is mixed in the free-shear layer from downstream. Our experimental data indicate that (16) is valid within an error of less than 5%.

In all numerical efforts to calculate the strength of the discrete vortex via (16), the position and initial velocity of the vortex are arbitrarily assigned. The present group is working on an interactive numerical approach which will allow the calculation of this necessary information. In the present paper we have taken the first steps towards measuring the flux of vorticity as well as the direction and rate with which vorticity is ejected into the flow.

Let Ω_c and y_c be an average of vorticity across a layer and the centroid of the vorticity profile respectively:

$$\Omega_c = \frac{1}{\delta} \int_0^\delta \Omega \, \mathrm{d}y, \tag{17}$$

$$y_c \Omega_c = \int_0^\delta \Omega y \, \mathrm{d}y. \tag{18}$$

Station no.	1	2	3	4	5	6
v_c/u_e	0.008	0.001	0.0071	0.0102	0.0156	0.0196
Station no.	7	8	9	10	11	12
v_c/u_e	0.0245	0.0286	0.0356	0.0426	0.0476	0.0538
Station no.	13	14	15	16	17	18
v_c/u_e	0.0599	0.0685	0.0745	0.0784	0.0848	0.0919

TABLE 1. The normal component of the velocity of vortex shedding.

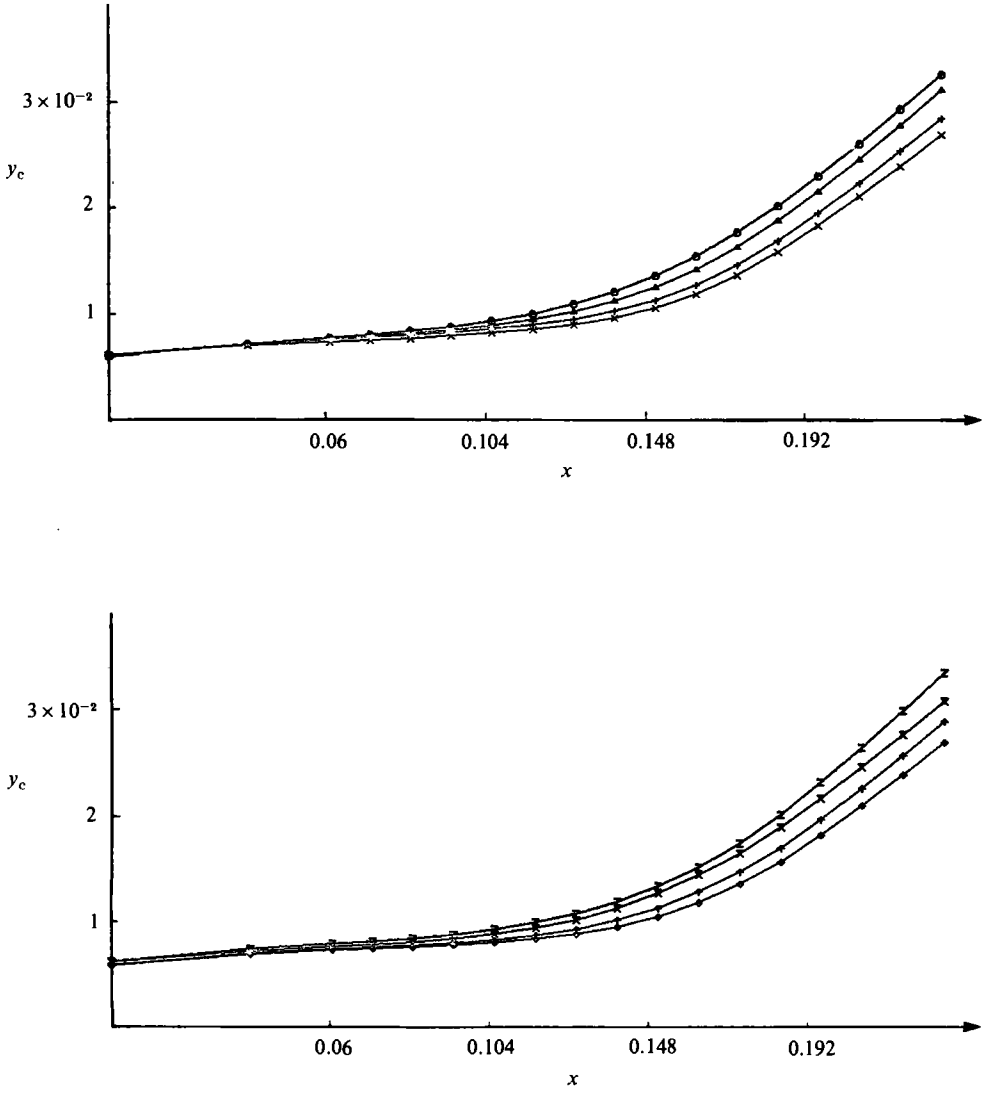

FIGURE 22. Centre of vorticity versus x and t (stations 1–18): ○, $t = \frac{1}{8}T$; ▲, $\frac{1}{4}T$; +, $\frac{3}{8}T$; x, $\frac{1}{2}T$; ◇, $\frac{5}{8}T$; ✕, $\frac{3}{4}T$; ↑, $\frac{7}{8}T$; z, $1T$.

The convection velocity of the vorticity could be defined as follows:

$$u_c = \frac{1}{\Omega_c} \int_0^\delta \Omega u \, dy, \tag{19}$$

$$v_c = \frac{1}{\Omega_c} \int_0^\delta \Omega v \, dy. \tag{20}$$

We have estimated all the above quantities based on our experimental data for many instances and found that the quantity u_c/u_e takes values in the attached as well as the separated domain which, in the mean, vary between 0.45 and 0.51. There is a small periodic fluctuation about this value which is at most equal to 0.08. In other words vorticity is shed with a velocity approximately equal to half of the edge velocity. This is a straightforward analytical result of (16) if one approximates vorticity by the quantity $\partial u/\partial y$. This finding therefore provides further evidence that the boundary-layer approximation is valid throughout separation.

The normal component of the velocity of vortex shedding, v_c/u_e, is about one order of magnitude smaller than u_c/u_e but increased monotonically with downstream distance. Its values are given in table 1.

Finally, the centre of vorticity defines a curve which could be termed the centre line of vorticity. Instantaneous positions of these curves are shown in figure 22. The behaviour of the vorticity centreline is very similar to the displacement thickness. To demonstrate this we have plotted the time variation of y_c at the 12th station in figure 20, where the displacement thickness variation is also shown.

7. Conclusions

Much argument and discussion has appeared in the literature on the controversy of coincidence or not of the points of zero skin friction and unsteady separation. The work presented in this paper is not intended to offer new evidence on this topic, simply because the amplitude of the unsteady oscillation is small. We did not observe any large-scale departures of the point of separation and the point of zero skin friction. However, it appears that the fluctuations of the free shear layer lead the other separation symptoms.

The reduced frequency of the outer oscillation was rather large. It therefore may appear that for small amplitudes and large frequencies the flow barely deviates from its mean. The motion then should be quasi-steady. This is not at all the case. Our results indicate deviations in the angle of separation, amplitude overshoots of the order of 500% and phase differences of the order of 100°.

The main contribution of this publication is a set of very careful measurements on a very thick measuring grid for a well-controlled separation. We offer here a well-documented case with measurements of both instantaneous velocity components well upstream and downstream of the point of separation.

We have examined carefully the terms of the Navier–Stokes equations, calculated using our experimental data. We conclude here that, in agreement with recently published analytical results on the topic, the boundary-layer approximation is valid, within an error of 10%, up to and beyond separation. Moreover, and again as predicted by the late Professor K. Stewartson (Stewartson 1974), the level of approximation does not change if one refers to coordinates aligned with the displacement thickness of the boundary layer. In the terminology of computations,

the boundary-layer approximation should be valid if the calculation is interacted with the outer flow. These statements are true for steady as well as unsteady flow.

A careful observation of figure 22 indicates that the vorticity centrelines curve smoothly as the flow turns away from the wall but then realign themselves along very nearly straight lines. Tangents to these straight lines project back and hit the wall. These points provide an arbitrary but reasonable definition of the point of separation. It remains to prove that this point would be independent of the Reynolds number. Incidentally, based on this definition, the excursions of the point of separation are contained between the points $x = 0.109$ and 0.114. In other words, for the high-frequency oscillations under consideration, the point of separation is rather insensitive to periodic disturbances, in agreement with the findings of Despard & Miller (1971).

The amount of our actual experimental data is at least 10 times more than we could fit into the few figures contained in this paper. The reader will find more detailed information in the Ph.D. dissertation of one of us (Mathioulakis 1985). We will also be happy to supply to anyone who requests them all the data that we obtained on tape.

This work was supported by the US Air Force Office of Scientific Research Grant No. 82-0228 and was monitored by Major Michael S. Francis.

REFERENCES

ARENA, A. V. & MUELLER, T. J. 1978 Visualization of separation and subsequent transition near the leading edge of an airfoil. *NASA Conf.* 2045, Part 2, Paper 35.

BERNAL, L. P. 1981 The coherent structure of turbulent mixing layers. I. Similarity of the primary vortex structure. II. Secondary streamwise vortex structure. Ph.D. thesis, California Institute of Technology, Pasadena, CA.

BIRKHOFF, G. 1953 Formation of vortex streets. *J. Appl. Phys.* **24**, 98–103.

CARR, L. W., MCALISTER, K. W. & MCCROSKEY, W. J. 1977 Analysis of the development of dynamic stall based on oscillating airfoil experiments. NASA *Tech. Note* D-8382.

CLEMENTS, R. R. 1973 An inviscid model of two-dimensional vortex shedding. *J. Fluid Mech.* **57**, 321–336.

COUSTEIX, J. 1986 Three-dimensional and unsteady boundary-layer computations. *Ann. Rev. Fluid Mech.* **18**, 173–196.

DESPARD, R. A. & MILLER, J. A. 1971 Separation in oscillating boundary-layer flows. *J. Fluid Mech.* **47**, 21–31.

DIDDEN, N. & HO, C.-M. 1985 Unsteady separation in a boundary layer produced by an impinging jet. *J. Fluid Mech.* **160**, 235–256.

DRYDEN, H. L. & ABBOTT, I. H. 1948 The design of low-turbulence wind tunnels. *NACA Tech. Note* 1755.

FAGE, A. & JOHANSEN, F. C. 1927 The flow of air behind an inclined flat plate of infinite span. *Aero. Res. Counc. R & M* **1104**, 81–106.

GERRARD, J. H. 1978 The wakes of cylindrical bluff bodies at low Reynolds number. *Phil. Trans. R. Soc. Lond.* A**288**, 351–382.

HALL, P. & SMITH, F. T. 1984 On the effects of nonparallelism, three dimensionality, and more interaction on nonlinear boundary-layer stability. *Stud. Appl. Maths* **70**, 91–120.

HO, C.-M. & HUERRE, P. 1984 Perturbed free-shear layers. *Ann. Rev. Fluid Mech.* **16**, 365–424.

KONRAD, J. H. 1976 An experimental investigation of mixing in two-dimensional turbulent shear flows with applications to diffusion-limited chemical reactions. *Project SQUID Tech. Rep.* CIT-8-PU.

KOROMILAS, C. A. & TELIONIS, D. P. 1980 Unsteady laminar separation – an experimental study. *J. Fluid Mech.* **95**, 347–384.

LIGHTHILL, M. J. 1954 The response of laminar skin friction and heat transfer to fluctuations in the stream velocity. *Proc. R. Soc., Lond.* A**224**, 1–23.

LOEHRKE, R. I. & NAGIB, H. M. 1976 Control of free-stream turbulence by means of honeycombs: a balance between suppression and generation. *Trans. ASME* I: *J. Fluids Engng* **98**, 343–353.

LUDWIG, G. R. 1964 An experimental investigation of laminar separation from a moving wall. *AIAA Paper* 64–6.

MATHIOULAKIS, D. S. 1985 Vorticity shedding over two-dimensional bodies. Ph.D. thesis, Virginia Polytechnic Institute & State University.

MATHIOULAKIS, D. S. & TELIONIS, D. P. 1985 Velocity and vorticity measurements around laminar separation. In *Numerical and Physical Aspects of Aerodynamic Flows* (ed. T. Cebeci), pp. 7.3–7.12. California State University

MCCROSKEY, W. J. 1971 Dynamic stall on a helicopter rotor blade. *Proc. SQUID Workshop, Atlanta* (ed. F. J. Marshall), pp. 346–350.

MCCROSKEY, W. J. 1977 Some current research in unsteady fluid dynamics – the 1976 Freeman Scholar Lecture. *Trans. ASME* I: *J. Fluids Engng* **99**, 8–38.

MEZARIS, T. B. & TELIONIS, D. P. 1980 Visualization and measurement of separating oscillatory laminar flow. *AIAA Paper* 80–1420.

MEZARIS, T. B., TELIONIS, D. P., BARBI, C. & JONES, G. S. 1987 Separation and wake of pulsating laminar flow. *Proc. R. Soc. Lond.* (in press).

MICHALKE, A. 1965 On spatially growing disturbances in an inviscid shear layer. *J. Fluid Mech.* **23**, 521–544.

MOORE, F. K. 1958 On the separation of the unsteady boundary layer. In *Boundary Layer Research* (ed. H. Görtler), pp. 296–310. Springer.

ROSHKO, A. 1953 On the development of turbulent wakes from vortex streets. *NACA Tech. Note* 2913.

ROSHKO, A. 1954 On the drag and shedding frequency of two-dimensional bluff bodies. *NACA Tech. Note* 3169.

ROTT, N. 1956 Unsteady viscous flow in the vicinity of a stagnation point. *Q. Appl. Maths* **13**, 444–451.

RUITER, G. H., NAGIB, H. M. & FEJER, A. A. 1971 Unsteady boundary-layer separation over oscillating airfoils. *Proc. SQUID Workshop, Atlanta* (ed. F. J. Marshall) pp. 423–425.

SAFFMAN, P. G. & SCHATZMAN, J. C. 1982 An inviscid model for the vortex-street wake. *J. Fluid Mech.* **122**, 467–486.

SARPKAYA, T. 1975 An inviscid model of two-dimensional vortex shedding for transient and asymptotically steady separated flow over an inclined plate. *J. Fluid Mech.* **68**, 109–128.

SCHRAUB, F. A., KLINE, S. J., HENRY, J., RUNSTADLER, P. W. & LITTEL, A. 1965 Use of hydrogen bubbles for quantitative determination of time dependent velocity fields in low-speed water flows. *Trans. ASME* D: *J. Basic Engng* **87**, 429–444.

SCHUBAUER, G. B., SPANGENBERG, W. G. & KLEBANOFF, P. S. 1948 Aerodynamic characteristics of damping screens. NASA *Tech. Note* 2001.

SEARS, W. R. 1956 Some recent developments in airfoil theory. *J. Aero. Sci.* **23**, 490–499.

SEARS, W. R. & TELIONIS, D. P. 1975 Boundary-layer separation in unsteady flow. *SIAM J. Appl. Maths* **28**, 215–235.

SHEN, S. F. 1978 Unsteady separation according to the boundary-layer equation. *Adv. Appl. Mech.* **18**, 177–220.

SIMPSON, R. L. 1981 A review of some phenomena in turbulent flow separation. *Trans. ASME* I: *J. Fluids Engng* **103**, 20–33.

SMITH, F. T. 1985 Nonlinear effects and non-parallel flows; the collapse of separating motion. *United Technologies Research Center, Engng Rep.* UTRC85–55.

SMITH, F. T. 1986 Steady and unsteady boundary-layer separation. *Ann. Rev. Fluid Mech.* **18**, 197–220.

STEWARTSON, K. 1974 Multi-structured boundary layers on flat plates and related bodies. *Adv. Appl. Mech.* **14**, 145–239.

TAN-ATICHAT, J., NAGIB, H. M. & LOEHRKE, R. I. 1982 Interaction of free-stream turbulence with screens and grids: a balance between turbulence scales. *J. Fluid Mech.* **114**, 501–528.

TELIONIS, D. P. 1979 Review – unsteady boundary layers, separated and attached. *Trans. ASME* I: *J. Fluids Engng* **101**, 29–43.

TELIONIS, D. P. & KOROMILAS, C. P. 1978 Flow visualization of transient and oscillatory separating laminar flows. In *Nonsteady Fluid Dynamics* (ed. D. E. Crow & J. A. Miller), pp. 21–32. ASME.

TELIONIS, D. P. & MATHIOULAKIS, D. S. 1984 On the shedding of vorticity at separation. In *Unsteady Separated Flows* (ed. M. W. Luttges), pp. 106–116. AFOSR, SRL, University of Colorado.

TELIONIS, D. P., MATHIOULAKIS, D. S., KIM, B. K. & JONES, G. J. 1986 Calibration of the ESM Water Tunnel. *VPI&SU Eng. Rep. VPI-E*-86-23.

TELIONIS, D. P. & ROMANIUK, M. S. 1978 Velocity and temperature streaming in oscillating boundary layers. *AIAA. J.* **16**, 488–495.

TSAHALIS, D. TH. & TELIONIS, D. P. 1974 Oscillating laminar boundary layers and unsteady separation. *AIAA J.* **12**, 1469–1475.

VARTY, R. L. & CURRIE, I. G. 1984 Measurements near a laminar separation point. *J. Fluid Mech.* **138**, 1–19.

VIDAL, J. R. 1959 Research on rotating stall in axial-flow compressors, part III. *WADC TR*-59-75.

WEI, T. & SMITH, C. R. 1986 Secondary vortices in the wake of circular cylinders. *J. Fluid Mech.* **169**, 513–533.

WÉRLÉ, H. 1973 Hydrodynamic flow visualization. *Ann. Rev. Fluid Mech.* **5**, 361–382.

WIGELAND, R. A., AHMED, M. & NAGIB, H. M. 1978 Management of swirling flows with application to wind tunnel design. *AIAA J.* **16**, 1125–1131.

WILLIAMS, J. C. 1977 Incompressible boundary layer separation. *Ann. Rev. Fluid Mech.* **9**, 113–144.

WINKELMANN, A. E. & BARLOW, J. B. 1980 Flowfield model for a rectangular planform wing beyond stall. *AIAA J.* **18**, 1006–1008.

WINKELMANN, A. E., NGO, H. T. & DESAIFE, R. C. 1982 Some observation of separating flow on finite wing. *AIAA Paper* 82-0346.